# Electrodynamic processes in colliding beams of high-energy particles

**V. G. Gorshkov**
*A. F. Ioffe Physico-technical Institute,*
*USSR Academy of Sciences*
Usp. Fiz. Nauk **110**, 45-75 (May 1973)

A classification is presented for the processes in quantum electrodynamics at high energy. The classification is based not on perturbation theory but on the character of the asymptotic behavior of the amplitudes and cross sections at high energy. A simple procedure is described for finding the asymptotic forms of the amplitudes of different processes from the form of the intermediate state in the crossing channel. A review is presented of the theoretical results for processes with cross sections that do not decrease with increasing energy. Double-logarithmic asymptotic expressions are obtained for processes with cross sections that decrease with increasing energy by summing the principle terms of the perturbation-theory series.

## CONTENTS

1. Introduction . . . . . 322
2. Kinematics and Dynamics of High Energies . . . . . 324
3. Processes with Cross Sections that do not Decrease with Increasing Energy. . . 326
4. Processes with Cross Sections that Decrease with Increasing Energy. . . . . 331
Bibliography. . . . . 337

## 1. INTRODUCTION

At low energies, all quantum-electrodynamic processes are usually classified on the basis of perturbation theory with respect to the number of powers of the fine-structure constant $\alpha = 1/137$ used to determine the cross sections of these processes. The simplest two-particle processes, such as scattering of electrons by electrons and positrons, scattering of photons by electrons, and annihilation of an electron-positron pair into a photon-and-muon pair, take place in second order of perturbation theory and have a cross section on the order of $r_0^2 = \alpha^2/m^2 \sim 10^{-25}$ cm$^2$. In multiparticle electrodynamic processes, each additional emitted particle gives rise to an extra factor $\alpha$ in the cross section. Therefore processes with large numbers of final particles are in general not considered in low-energy quantum electrodynamics. The higher-order perturbation theories for the amplitudes of two-particle processes contain the so-called radiative corrections. At low energies, it suffices to calculate only the first radiative correction, which amounts to no more than 1%.

At high energies greatly exceeding the rest energy of the electron or muon, the traditional classification of the quantum-electrodynamics processes in the spirit of perturbation theory is not satisfactory. The cross sections at high energies are determined mainly not by the number of powers of $\alpha$, but by the character of the dependence of the amplitudes on the cross sections and on the energy.

The development of high-energy physics in recent years has led to the recognition of the fact that the asymptotic forms of the total cross sections of different processes, and also of the differential cross sections at small angles and at angles close to 180° are determined by the character of the intermediate states of the crossing channels of the reaction. In hadron physics these states are the Regge poles and cuts with complex values of the orbital angular momentum[1]. In electrodynamics, by virtue of the presence of small coupling constants, the singularities of the crossing channels are determined by the usual particles—photons, electrons, and muons[2,3]. Reggeization of these states can occur in higher orders of perturbation theory[3-5].

A procedure for determining the asymptotic behavior of electrodynamic processes can be distinctly formulated. To this end we introduce the usual energy and angular invariants of the processes

$$s=(p_1+p_2)^2\approx 2p_1p_2\gg m^2,\quad t=(p_1-p_1')^2,\quad u=(p_1-p_2')^2, \tag{1}$$

where $p_1$, $p_2$ and $p_1'$, $p_2'$ are the 4-momenta of the initial and final particles of the reaction shown in Fig. 1a. In the c.m.s. ($\mathbf{p}_1 = -\mathbf{p}_2$), the invariants (1) take the form[1)]

$$s = 4E^2,\quad t = -s\,(1-\cos\vartheta)/2,\quad u = -s\,(1+\cos\vartheta)/2, \tag{2}$$

where E and $\vartheta$ are the energy and scattering angle of the particles. We shall therefore call the invariant s the squared energy and the invariants t and u the squared transferred momenta. The direct channel of the reaction with the initial particles that make up the invariant s will be called the s-channel. The crossing channels with initial particles making up the invariants t and u will be called the t- and u-channels, respectively. In the case of multiparticle processes, we introduce several momentum transfers made up of the momenta of the initial and final particles, $t_i = q_i^2$ (Fig. 1b; see also Fig. 3 below) and the partial energies of the process $s_{ik}^{1/2}$, made up of the momenta of the final particles:

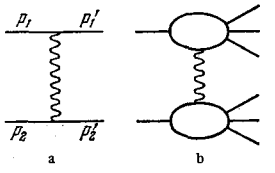


FIG. 1.

  

$$s_{ik} = \left(\sum_{n=i}^{k} p_n\right)^2. \qquad (3)$$

The processes whose amplitudes can be separated into two parts in the t-channel by intersecting only the photon lines (Fig. 1) have total cross sections that do not decrease with increasing energy[2,3]. The main contribution to the cross section of the process is made by diagrams with the smallest number of parallel photons in the t-channel[2)]. Diagrams with an increasing number of parallel photons have the same energy behavior and constitute, just as in the case of low energies, small radiative corrections to the principal diagrams. In all the processes in colliding beams where the amplitudes contain photon splittings in the t-channel, one intermediate photon is possible. However, in processes such as the Compton effect and scattering of light by light (Fig. 2), the number of photons in the t-channel can be only even, by virtue of C-parity conservation. We note that both diagrams of the Delbruck type (see Figs. 2a and 2b), which make the principal contribution to the constant cross section, are radiative corrections to the diagrams of Figs. 2c and 2d at low energies. With increasing energy, the contribution of the diagrams of Figs. 2c and 2d, which have no photons in the intermediate state of the t-channel, decreases rapidly and becomes smaller than the contribution of the diagrams of Figs. 2a and 2b at $s^{1/2} \sim 3$ GeV[6,7].

In addition to having power-law constancy, the electrodynamic cross sections in Fig. 1b can also have a logarithmic growth of some definite degree. The degree of logarithmic growth is in the general case $n-1$, where n is the number of successive intermediate photons in the t-channel in Fig. 3[8,9]. In addition, if the initial particle, together with the final particle and the intermediate photon in the t-channel, makes up the very simple vertex of Fig. 3b, then one more (Weizsacker) logarithm[10-12] appears for this outermost photon. Thus, the maximum degree of the logarithm, with allowance for the two possible outermost logarithms, is $(n-1)+2$. All that drops out from the presented scheme is the process of elastic scattering of electrons by electrons and positrons (Fig. 1a), the total cross section of which is infinite at any energy. It is easy to see that for each logarithm (excluding the outermost Weizsacker logarithms) there is at least one factor $\alpha$[28,9]. The quantity $\alpha^2\ln(s/m^2)$ is small at all the attainable energies. Therefore the cross sections of the processes containing t-channel photon splittings (Fig. 3) decrease with increasing number of final particles, and they can be classified on the basis of perturbation theory. The non-decreasing total cross section of the processes in Figs. 1 and 3 is due to the small scattering angles $\vartheta \sim m/s^{1/2}$, when the momentum transferred to the intermediate photon is $t \sim m^2$. The differential cross sections of any process in large-angle scattering, when all the momentum transfers $t_i$ are nearly equal to s, decrease linearly with increasing s. Therefore the region of large $t_i \sim s$ makes no contribution to the total cross section of the processes in Fig. 1b. Processes that do not decrease with increasing energy are considered in Chap. 3.

Processes having no photon splittings in the t-channel decrease linearly with increasing s at all scattering angles. The total cross sections of these processes also decrease. However, a new phenomenon appears for processes of this type[13,14]. The radiative corrections

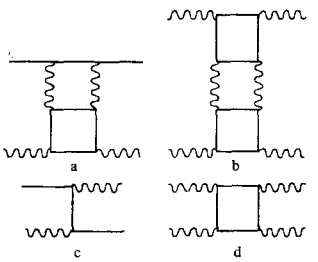

FIG. 2.

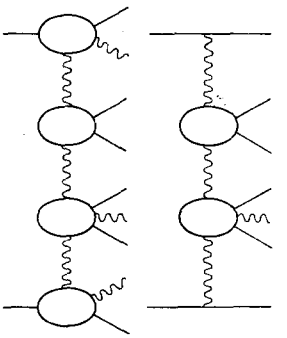

FIG. 3.

connected with the intermediate photons for these processes contain, for each power of $\alpha$, the logarithm raised to a maximum power of two (see Chap. 2). The resultant parameter for the perturbation-theory expansion $(\alpha/\pi)\ln^2(s/m^2)$ turns out to be of the order of unity at energies $s^{1/2} \sim 10$ GeV. The amplitudes of the processes are now determined by the sum of all the radiative corrections containing the parameter $(\alpha/\pi)\ln^2(s/m^2)$, which differs significantly at high energies from the Born term (the first-order perturbation-theory approximation). The total cross sections of the processes with emission of an additional number of photons also contain the parameter $(\alpha/\pi)\ln^2(s/m^2)$ for each emitted photon. These processes, which appear in different orders of perturbation theory, therefore have cross sections of the same order at sufficiently high energies. At very high energies, when $(\alpha/\pi)\ln^2(s/m^2) \gg 1$, the cross section of the processes with emission of a specified number of photons can become larger than the cross sections of the processes with emission of a smaller number of photons. Thus, three-photon annihilation of an electron-positron pair exceeds the two-photon annihilation at energies $s^{1/2} \gtrsim 50$ GeV and $\omega_{min} \sim m$[15].

Double-logarithmic terms come in various types[3]. In charged-particle scattering through large angles $\vartheta \sim 1$, a double-logarithmic contribution comes from the real and virtual Bremsstrahlung photons, which are classical in nature and satisfy a Poisson distribution[14,16-18]. In the case of poor energy resolution ($\Delta E \sim E$) or angular resolution ($\Delta\vartheta \sim \vartheta$), when a large number of real Bremsstrahlung photons of high energy is emitted, there is no double-logarithmic contribution from these photons owing to their Poisson distribution.

In scattering through small angles or angles close to 180°, a double-logarithmic contribution that has no classical analog is made by photons[3,14]. This contribution does not have a Poisson distribution and is connected with the fact that the electron has a half-integer spin[3,14]. Processes with decreasing cross sections are considered in Chap. 4.

It appears that high electron energies $s^{1/2} \sim 1$—10 GeV are presently attainable and will be attainable in the nearest future only in colliding-beam installations[19,20], since the corresponding energies in the laboratory system $E_{lab} \approx s/2m$ are of the order of $10^3$—$10^5$ GeV and are temporarily unattainable with an accelerator having an immobile target. We shall henceforth consider therefore only processes that take place in colliding-beam accelerators, with an electron-electron or electron-positron pair as the initial particles.

## 2. KINEMATICS AND DYNAMICS OF HIGH ENERGIES

In order to explain the character of the behavior of the cross sections of electrodynamic processes at high energies relative to changes of the invariants s and t, we consider in detail the kinematics and dynamics of the processes in the region $s \gg m^2$.

a) **Kinematics. Phase volume.** The chief purpose of the present section is to obtain an expression for the phase volume (see formulas (17), (21), and (24) below), and also to acquaint the reader with the Sudakov variables, which we shall use repeatedly in what follows.

We introduce the usual invariant amplitude for the production of n final particles, M, normalized by the condition

$$S = 1 + (2\pi)^4 i\delta(p_1 + p_2 - \sum_i p_i')(2E_1 \cdot 2E_2)^{-1/2}[\prod_i (2E_i')^{1/2}]^{-1} M^n, \quad (4)$$

where $p_i$, $E_i$ and $p_i'$, $E_i'$ are the momenta and energy of the initial and final particles. The normalization volume is set equal to unity. For the cross section for the production of n final particles we obtain the expression

$$d\sigma_n = (2s)^{-1} \sum_j |M^n|^2 d\Gamma_n, \quad (5)$$

$$d\Gamma_n = \prod_{j=1}^{n} [d^3p_j'/(2\pi)^3 2E_j'] (2\pi)^4 \delta(p_1 + p_2 - \sum_{j=1}^{n} p_j'). \quad (6)$$

The symbol $\sum_j$ in (5) denotes summation over the spin states of the final particles; in addition, averaging over the polarization of the initial particles is implied in (5). These operations can be carried out in the expressions (5) and (6) for the cross section with the aid of the known formulas

$$A^\nu \equiv \sum_\lambda \varepsilon_\mu^\lambda \varepsilon_\nu^\lambda = \delta_{\mu\nu} - (k_\mu k_\nu/k^2), \quad (7)$$

$$A^e \equiv \sum_\lambda u_p^\lambda \bar{u}_p^\lambda = \hat{p} + m, \ \hat{p} = \gamma_\mu p_\mu, \quad (8)$$

where $\epsilon_\mu$ and $u_p$ are the polarization functions of a photon with momentum k and an electron with momentum p (the Dirac bispinor). By virtue of the definition (4), the electronic functions are normalized by the condition

$$j_\mu = \bar{u}_p \gamma_\mu u_p = 2p_\mu, \ \bar{u}_p u_p = 2m. \quad (9)$$

The current-conservation condition, as usual, makes it possible to discard the last term of (7).

Noting that

$$d^3p/(2\pi)^3 2E = [d^4p/(2\pi)^4] \cdot 2\pi\delta(p^2 - m^2)|_{E>0}, \quad (10)$$

we can rewrite the phase volume (6) in the form

$$d\Gamma_n = \prod_{j=1}^{n-1} \{[d^4p/(2\pi)^4] \cdot 2\pi\delta(p_j^2 - m^2)\} 2\pi\delta(p_n^2 - m^2). \quad (11)$$

Taking (11), (7), and (8) into account, we note that $M^n M^{n+} d\Gamma_n$ is the amplitude of the diagram of Fig. 4[14,21]. The left-hand side of Fig. 4 is the amplitude $M^n$, and the right-hand side is the complex-conjugate amplitude $M^{n+}$, in which the directions of all the charged lines are reversed[3]. All the intermediate lines of the amplitudes $M^n$ and $M^{n+}$ correspond, as before, to electron or photon propagators, and all final particles correspond to intermediate crossed lines joining the amplitudes $M^n$ with $M^{n+}$—the factors $2\pi A_j \delta(p_j^2 - m_j^2)$. These factors differ from the propagators in that the pole $(p_j^2 - m_j^2 + i\epsilon)^{-1}$ is replaced by double its imaginary (absorption) part $2\pi\delta(p_j^2 - m_j^2)$. Generally speaking, the

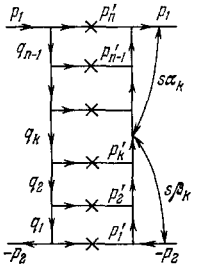

FIG. 4.

diagram of Fig. 4 comprises, after integration over all the invariants contained in (11), an incomplete doubled imaginary (absorption) part of the amplitude of the forward elastic scattering, $\mathrm{Im}^n_{ela}(0)$[24,25]. The total imaginary part appears after summation over all the possible number of the final particles, $\mathrm{Im}\, M_{ela} = \sum_n \mathrm{Im}\, M^n_{ela}$. It is connected with the total cross section by the optical theorem $\sigma = \mathrm{Im}\, M_{ela}(0)/s$.

We transform the phase volume, separating those variables the integration with respect to which can lead to large logarithms[4] $\ln(s/m^2)$. These variables are obviously the energies of the final particles and the momentum transfers, which depend on the angles $\vartheta$ between the momenta of the emitted particles and the beam directions. The angle variables in the plane perpendicular to the beam do not depend on the energy in perturbation theory. Thus, for each of the final particles except two we obtain, generally speaking, not more than two large logarithms. The remaining two particles can give rise to only one logarithm each. In a two-particle reaction, this logarithm arises upon integration with respect to the single transferred momentum. Altogether, consequently, we can obtain at most $2n - 3$ large logarithms after integrating over the phase volume of n final particles[26].

Integration over the final particles is conveniently carried out by changing over from the variables $p_j'$ to the momentum transfers $-q_j = p_2 - \sum_{i=1}^{j} p_i'$ (see Fig. 4). We resolve $q_j$, following Sudakov[13], into invariant longitudinal and transverse parts:

$$q = p_1\beta - p_2\alpha + q_\perp, \quad p_1 q_\perp = p_2 q_\perp = 0, \quad (12)$$

$$-t = q^2 = -s\alpha\beta + q_\perp^2, \quad (13)$$

$$d^4q = (s/2)\, d\alpha\, d\beta\, d^2q_\perp = \pi\, (s/2)\, d\alpha\, d\beta\, dt\, (d\varphi/2\pi). \quad (14)$$

In the c.m.s., the component q is a spatial vector perpendicular to the line of motion of the beams, and therefore $q_\perp^2 < 0$. The quantities $s\beta_k (s\alpha_k)$ have a simple physical meaning. They coincide asymptotically with the energy invariants $s_{1k} (s_{kn})$ of parts of the amplitude in Fig. 4 with the momenta of the limiting particles $p_2$ and $q_k$ ($p_1$ and $q_k$). Indeed,

$$s_{1k} = (\sum_{i=1}^{k} p_i')^2 = (p_2 + q_k)^2 = s\beta_k - 2m^2\alpha_k + m^2 - t_k \approx s\beta_k \gg m^2, \ t_k,$$
$$s_{kn} = (\sum_{i=k+1}^{n} p_i')^2 = (p_1 - q_k)^2 = s\alpha_k - 2m^2\beta_k + m^2 - t_k \approx s\alpha_k \gg m^2, \ t_k. \quad (15)$$

The quantity $s/2m$ (1) is the energy of a particle with momentum $p_1$ in the rest system of a particle with momentum $p_2 = 0$. Analogously, the quantities $s\beta_k/2m$ ($s\alpha_k/2m$) are the energies of particles with momentum

$q_k$ in the rest system of a particle with momentum $p_2$ = 0 ($p_1 = 0$).

From the condition that the energies of the final particles be positive, we obtain

$$1 > \beta_{n-1} > \beta_{n-2} > \ldots > \beta_2 > \beta_1 > 0, \quad (16a)$$

$$1 > \alpha_1 > \alpha_2 > \ldots > \alpha_{n-2} > \alpha_{n-1} > 0. \quad (16b)$$

The conditions (16) are obvious from the point of view of the just performed interpretation of $s\beta$ and $s\alpha$. Indeed, in the rest system of the particle 1, $p_1 = 0$ (the rest system of the particle 2, $p_2 = 0$), the energies of the intermediate particles should increase (decrease) on going from particle 2 to particle 1 in Fig. 4.

In the region of the maximal logarithmic behavior, none of the variables can be of the order of another, for otherwise we lose the logarithms with respect to one of these variables. This condition greatly simplifies the manipulation. All the inequalities in (16) must thus be understood in the enhanced sense. In all the $\delta$ functions of (11), it suffices to retain only the product of the largest $\alpha_i$ by the largest $\alpha_i$. In the case of the ladder amplitude in Fig. 4 (which depends on the momentum transfers $t_i$) we can replace $d\varphi/2\pi$ in (14) by unity. Integrating the $\delta$ functions in (11) with respect to $d\alpha_i$, we obtain

$$d\Gamma_n = 2\pi\,[dt_{n-1}/(4\pi)^2 s] \prod_{j=n-1}^{2} ds\beta_j\,[dt_{j-1}/(4\pi)^2 s\beta_j]. \quad (17)$$

The limitations on the variables $s\beta_j$ are determined by the inequalities (16a). The limitations on the variables $t_j$ follow from the vanishing of the arguments of the $\delta$ functions (11) after their integration with respect to $d\alpha_i$ and from the definition (13), which by virtue of $q_\perp^2 < 0$ and $s\alpha\beta > 0$ should take the form of the inequality

$$t > s\alpha\beta \quad \text{or} \quad t \gg s\alpha\beta. \quad (18)$$

The resultant limitations on the variables $t_j$ can be expressed in the form of a chain of inequalities[13]

$$1 = t_1/s\beta_1 \gg t_2/s\beta_2 \gg \ldots \gg t_{n-1}/s\beta_{n-1} \gg m^2/s. \quad (19)$$

Thus, the final limits of variation of the phase-volume variables (17) are bounded by the conditions (16a) and (19).

The expression for the phase volume (17) has a simple interpretation. The two-particle phase volume is equal to

$$d\Gamma_2 = 2\pi\, dt/(4\pi)^2 s. \quad (20)$$

The multiparticle phase volume (17) is obtained in the following manner. First we calculate with formula (20) the two-particle phase volume of the block of the cross section bounded by particles with momenta $p_2$ and $q_2$ with the energy invariant $s_{12} = s\beta_2$. Formula (20) is then used to calculate the two-particle phase volume of the block of the section bounded by the particles with momenta $p_2$ and $q_3$ with energy invariant $s_{13} = s\beta_3$, with the final particles 1′ and 2′ playing the role of one particle with an effective mass equal to $s_{12} = s\beta_2$, with respect to which it is necessary to integrate within the obvious limits $s\beta_3 \gg s\beta_2 \gg m^2$ (see (16a)), etc. The last differential takes the form of a two-particle phase volume for the entire cross section, in which the role of the first particle is assumed by the entire block of the cross section with $n - 1$ final particles and effective mass $s\beta_{n-1}$, with respect to which the integration is carried out up to the total energy s. The presented interpretation of the phase volume can be expressed mathematically in the form of the recurrence relation

$$d\Gamma_n(s, t) = [dt'/(4\pi)^2 s]\, ds'\, d\Gamma_{n-1}(s', t'), \quad (21)$$

$$s > s', \quad t/s < t'/s', \quad d\Gamma_1(s, t) = 2\pi\delta(s - t), \quad (22)$$

$$d\Gamma_n \equiv d\Gamma_n(s, m^2). \quad (23)$$

The expression for the single-particle phase volume (22) is valid at $t \gtrsim m^2$; at $t \ll m^2$, the zero value of the argument of the $\delta$ function (22) corresponds to equality (15).

On the basis of the foregoing interpretation of the phase volume, we can rewrite the expression for (21) in one more manner. We choose some cell in Fig. 4 with number k, and break up the diagram for the cross section in Fig. 4 into two blocks—left-hand and right-hand relative to the cell k. Then the phase volume of the entire process can be expressed in terms of the phase volumes of these blocks in the form

$$d\Gamma_n = (2\pi)^{-1}\, d\Gamma_{n-k-1}(s_{1k}, t_k)\, ds_{1k}\, [dt_k/(4\pi)^2 s]\, ds_{kn} d\Gamma_k(s_{kn}, t_k) \quad (s_{1k}, s_{kn} \ll s). \quad (24)$$

This expression has the form of a two-particle phase volume, where the left-hand block with effective mass $s_{1k}$ assumes the role of the first particle, and the right-hand block with effective mass $s_{kn}$ the role of the second particle. Formula (24) can be obtained directly by integrating the $\delta$ function with respect to $d\beta$ from above to the k-th cell and with respect to $d\alpha$ downward starting with the k-th cell.

b) **Dynamics. Power-law asymptotic forms of the amplitudes and the cross sections.** The purpose of this section is to obtain formulas for the asymptotic amplitudes (28), (29), and (30). Let us examine the dynamics connected with the behavior of the amplitudes M at high energy. In the case when all the momentum transfers $t_i$ are large, $t_i \sim s$, the dimensionless quantity $|M|^2 d\Gamma$ [Eq. (6)] should be of the order of unity, since M is described in the Born approximation by a set of simple poles with respect to different invariants[5)]. It follows from this that all the cross sections (5) for the large-angle scattering and production of particles are of the order of 1/s, i.e., they decrease with increasing energy.

This is not the case if the momentum transfers $q_i^2 = t_i$ are small, $t_i \lesssim m^2$. In this case the behavior of the amplitude depends on the spin of the particles with momentum $q_i$, exchange of which takes place in the t-channel. Let us explain the power-law (in s) dependence of the amplitude on the spin of the intermediate particles in the t-channel, disregarding the possible logarithms for the time being.

We consider the simplest Feynman pole diagram Fig. 1a, with the photon in the intermediate state of the t-channel. At small $t \lesssim m^2$, the momenta of the initial and scattered particles can be regarded as equal, $p_1 \approx p_1'$, $p_2 \approx p_2'$. The currents of the transitions of particles 1 and 2 in Fig. 1a take the form (9)

$$\bar{u}_{p_1'}\gamma_\mu u_{p_1} = 2p_{1\mu}, \quad \bar{u}_{p_2'}\gamma_\mu u_{p_2} = 2p_{2\mu}.$$

The amplitude in Fig. 1a, taking (1) into account, is therefore

$$M_1 = 4\pi\alpha \cdot 2s/t. \quad (25)$$

From the point of view of the t-channel, where t is the energy, the dimensionless amplitude M (see Fig. 1a) with one photon in the intermediate state consists of one partial wave with $l = 1$ and should be of the form[1,6)]

$$M_1 = f_1(t)\, P_1(z) = f_1(t) \cdot 2s/t. \quad (26)$$

It follows from (25) that $f_1(t) = 4\pi\alpha$ at $t \sim m^2$. In the

case of exchange of a scalar particle, the amplitude would consist of a zero partial wave and would be proportional to a constant (the constant $\alpha$ in (25) has for scalar particles the dimensionality $m^2$ and there is no s in the numerator).

We consider now exchange of a spinor particle (Fig. 2c). At $t \sim m^2$, the propagator of the spinor particle, by virtue of the presence of the numerator (8), is proportional to $t^{1/2}$. The spinors $u_p$ of two electrons in the c.m.s. are proportional to $p^{1/2} \sim s^{1/4}$. For the entire amplitude (Fig. 2c) we obtain a value of the order of

$$M_{1/2} \sim s^{1/2}/t^{1/2}. \tag{27}$$

Thus, the amplitudes containing the exchange of one particle in the t-channel behave at $t \sim m^2$ like

$$M_\sigma \sim s^\sigma, \tag{28}$$

where $\sigma$ is the spin of the intermediate particle[1,2,27].

In the case of the exchange of two particles in the t-channel with spins $\sigma_1$ and $\sigma_2$ (wavy lines in Fig. 5), each of the amplitudes containing the wavy line behaves in accordance with (28). However, by virtue of the smallness of $t \sim m^2$, the phase volume of the integration over the closed loop is small, $d\Omega \sim \pi dt'/s \sim m^2/s$.[7] The general behavior of the amplitude (Fig. 5a) at small t is therefore given by[4,27,28]

$$M \sim s^{\sigma_1+\sigma_2-1}. \tag{29}$$

It is easy to generalize our analysis to include exchange of an arbitrary number of particles in the t-channel. The exchange of each particle will give a factor (22), and integration of each closed loop with respect to the phase volume will give a small quantity of order $m^2/s$. Therefore the general behavior of the amplitude following exchange of n particles with spins $\sigma_1$, $\sigma_2$, ..., $\sigma_n$ is given by[4,27,28]

$$M \sim s^{j_n}, \qquad j_n = \sum_{k=1}^{n}\sigma_k - (n-1) = \sum_{k=1}^{n}(\sigma_k - 1) + 1. \tag{30}$$

An amplitude behavior similar to (30) can also be obtained by substituting in Fig. 5 the entire amplitude (29) for one of the virtual particles in the t-channel, and using the same reasoning as in the derivation of formula (29).

Expressions (29) and (30) are also valid in the general case when the horizontal solid lines in Figs. 5a and 5b are replaced by the arbitrary amplitudes A and B of Figs. 5c and 5d, which contain right-hand and left-hand cuts with respect to their partial energies[28]. The asymptotic form of the entire amplitude of Fig. 5c or 5d will be determined by the maximum value of $j_n$ (30) from among all the sets of the intermediate particles in the t-channel, contained in the amplitude of Fig. 5c or 5d. Thus, we see from (30) that only exchange of photons (whose number is furthermore arbitrary) in the t-channel leads to an amplitude that increases linearly with increasing s, and consequently (see (5)) to a constant cross section. The total cross section is in this case also constant and is determined by the small $t \sim m^2$, corresponding to preferred emission of the reaction particles at very small angles $\vartheta \sim m/s^{1/2}$. On the other hand, the process cross sections determined by diagrams with one spinor particle in the t-channel will decrease with increasing energy. In the latter case of exchange of two spinor particles, small $t \sim m^2$ are not singled out, and the total cross section is determined by the region that leads to the maximum number of large logarithms.

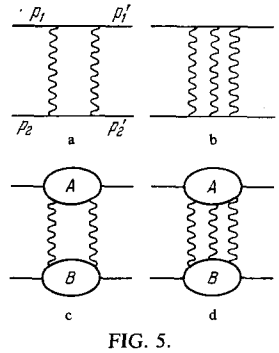

FIG. 5.

All the foregoing has pertained to the asymptotic form of the Feynman diagrams for the amplitudes of the processes. Formulas (29) and (30), with (5) taken into account, also describe correctly the asymptotics of the cross-section diagrams in Fig. 4 if the intermediate particles in the t-channel are taken to be only virtual particles that do not belong to the final reaction products; in other words, if in the t-channel one takes into account only the particles for the horizontal splitting of the diagram of Fig. 4, and not for oblique splitting, when the final real particles intersect.

The diagrams for the cross sections are more economical than the diagrams for the amplitudes. If the final particles are arranged in the form of horizontal parallel lines, we can investigate the horizontal splitting of the virtual particles in the t-channel and determine the asymptotic form of the cross section by means of formulas (29), (30), and (5). This immediately reveals amplitudes whose interference is small (see Fig. 9b below). Henceforth, whenever we refer to splitting in the t-channel or intermediate states in the diagrams for the cross sections, we shall have in mind only horizontal splittings and intermediate states connected with virtual particles.

## 3. PROCESSES WITH CROSS SECTIONS THAT DO NOT DECREASE WITH INCREASING ENERGY

a) **The Weizsacker-Williams formula.** We have seen that all the amplitudes containing exchanges of arbitrary numbers of parallel photons in the t-channel lead to a constant cross section. However, with each additional parallel photon, the amplitude is multiplied by a small quantity $\alpha$. This does not give rise to any logarithms[2,8].

Thus, the principal contribution to the cross section is made by diagrams containing the smallest number of parallel photons in the t-channel. For processes in colliding beams with constant cross section, exchange of one photon in the t-channel is always possible.

Let us consider the general form of the diagram for the cross section of the process containing exchange of one photon in the t-channel (Fig. 6). Using (24), we can express the cross section of Fig. 6 in the form

$$d\sigma = (2s)^{-1}(2\pi)^{-1} d\Gamma_1(s_1,t) f_{1\mu\nu}(s_1,t) ds_1 [dt/(4\pi)^2 s] t^{-2} ds_2 d\Gamma_2(s_2,t) f_{2\mu\nu}(s_2,t), \tag{31}$$

where $f_{i\mu\nu}$ are the squares of the moduli of the amplitudes of the upper and lower blocks, which are separated by the photon lines. The functions $f_{i\mu\nu}$ satisfy the gauge-invariance condition

$$q_\mu f_{i\mu\nu} = q_\nu f_{i\mu\nu} = 0, \quad t = q^2. \tag{32}$$

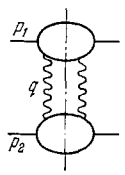

FIG. 6.

At t = 0 the functions $f_{i\mu\nu}$ are connected with the photoproduction-process cross section, determined by the lower or upper block of the diagram of Fig. 6:

$$(2s_i)^{-1}\overline{\varepsilon_\mu\varepsilon_\nu}\,d\Gamma_i f_{i\mu\nu}(s_i, 0) = d\sigma_i(s_i), \tag{33}$$

where the averaging over the polarizations of the photon can be carried out with the aid of formula (7).

Conditions (32) and (33) enable us to write for $f_{i\mu\nu}$, accurate to terms of order $t/q^2$, the expression

$$d\Gamma_i f_{i\mu\nu}(s_i, t) = \\ = 2d\sigma_i(s_i)\,[4p_{i\mu}p_{i\nu}(t/s_i) - 2(p_{i\mu}q_\nu + p_{i\nu}q_\mu) + \delta_{\mu\nu}s_i] \\ + b(\delta_{\mu\nu}q^2 - q_\mu q_\nu), \tag{34}$$

$$s_i = 2p_iq. \tag{35}$$

When (34) is substituted in (31), only the terms containing $p_{i\mu}p_{i\nu}$ in $f_{i\mu\nu}$ lead to the formation of the product $[2(p_1p_2)]^2 = s^2$, which is necessary to cancel out $s_2$ in the denominator of (31) and to obtain a constant cross section. The second and third terms in the square brackets of (34), as well as the quantity b, can therefore be discarded. We call attention to the appearance of the factor $t/s_i$ in the first principal term of (34). This factor leads to cancellation of one photon propagator in (31) and improves the convergence of the integral with respect to $s_i$. There is no factor $t/s_i$ if the block in Fig. 6 contains one electron or positron as the final particle. In this case, (33) is proportional to the $\delta$ function (22); as a result we have $t \approx s_i$ and the principal term of (34) is transformed into a product of two elementary currents (vertex parts) (9):

$$d\Gamma_2 f_{2\mu\nu} = 4\pi\alpha\cdot 4p_{2\mu}p_{2\nu}\cdot 2\pi\delta(s_2 + t,\ s_2 = 2p_2q = s\beta - 2m^2\alpha. \tag{36}$$

We have written out in (36) the exact expression for the argument of the $\delta$ function $(p_2 + q)^2 - m^2$ (15), which is valid for small $t \ll m^2$, since both formulas (34) and (36) have been derived accurate to terms of order $t/m^2$.

Substitution of formula (36) in both blocks of Fig. 6 yields the elastic-scattering cross section at small t (the Rutherford formula):

$$d\sigma = 4\pi\alpha^2\,dt/t^2, \quad m^2 \gg t \geqslant 0. \tag{37}$$

If only one of the blocks, e.g., the second, contains a single final particle, then a combination of (34) and (36) yields for the cross section (31) an expression of the type[10,11]

$$d\sigma = (\alpha/\pi)\,(dt/t)\,(ds_1/s_1)\,d\sigma_1(s_1), \tag{38}$$

$$m^2 \gg t \gtrsim m^2s_1^2/s^2. \tag{39}$$

The lower bound (39) on t follows from the $\delta$ function (36), the definition (15) and (35), and the condition $t \geq s\alpha\beta$ ($-q_\perp^2 \geq 0$) (18). As a result of cancellation of one photon propagator by the factor $t/s_1$ in (34), the cross section (38), in contrast to the elastic-scattering cross section (37), contains only a logarithmic differential with respect to t, which is called the Weizsacker-Williams logarithm. The principal contribution to the logarithmic integral with respect to t is given by the region (39), which thus determines the total cross section (38) with logarithmic accuracy.

In the case when both blocks of Fig. 6 are described by formula (34), the cross section (31) takes the form[2,8]

$$d\sigma = (4\pi^3)^{-1}\,dt\,(ds_1/s_1)\,d\sigma_1(s_1)\,(ds_2/s_2)\,d\sigma_2(s_2), \quad t \ll m^2. \tag{40}$$

In contrast to formula (38), formula (40) contains no logarithmic differential with respect to t, since both photon poles are cancelled out by the factors $t/s_i$ in (34). The total cross section, owing to the absence of the Weizsacker-Williams logarithm, is determined by the region $t \sim m^2$ and cannot be obtained from (40), which gives only its order of magnitude.

Formulas (38) and (40) have important features. If the cross section (31) has only one photon splitting in the t channel (Fig. 6), then the upper and lower blocks, which contain no photon lines, have decreasing cross sections. Therefore the principal contribution to the calculated total cross sections will be made by the region of small partial energies $s_1^{1/2}$, $s_2^{1/2} \lesssim m$, inasmuch as the integrals with respect to these variables converge rapidly with increasing $s_1$ and $s_2$, by virtue of the decrease of the cross sections $d\sigma_1$ and $d\sigma_2$.

Thus, if the cross section contains one photon splitting in the t-channel, then only one Weizsacker-Williams logarithm can arise.

Now let the cross section $d\sigma_1$ in (31) be itself determined by a diagram with photon splittings. In this case the cross section $d\sigma_1$ does not decrease with increasing energy $s_1^{1/2}$. Integration with respect to $s_1$ now leads to an additional logarithm. It is easily seen that the number of the logarithms that result in this case is $n - 1$, where n is the number of photon splittings in the t-channel plus one or two outermost Weizsacker-Williams logarithms, which arise in the case when one or both initial particles are coupled with the intermediate photons in the t-channel via the vertex parts (see Figs. 5a and 3b). The amplitude of the process is determined by the diagrams of Fig. 3, and the energy invariants $s_i$ of all the blocks containing no photon splittings in the t-channel turn out, just as in Fig. 6, to be of the order of $m^2$, i.e., these blocks are not under the asymptotic conditions.

b) **Elastic scattering.** We consider now all the processes that have cross sections that do not decrease with energy. The simplest such process is $e^+e^-$ or $e^-e^-$ scattering. The $e^+e^-$ scattering amplitude is described by the diagrams of Fig. 7a and 7b. In $e^-e^-$ scattering, diagram 7b is impossible. Instead, it is necessary to add to diagram 7a, in which the direction of the line with momentum $p_2$ should be reversed, the analogous diagram 7a′ with interchanged final lines $p_1'$ and $p_2'$. In $e^-e^-$ scattering, both diagrams have photons in the t-channel, whereas in $e^+e^-$ scattering, this property is possessed only by the diagram of Fig. 7a. The diagram of 7b is asymptotically small and can be discarded when small-angle scattering is taken into account. The cross section of these processes is represented by one diagram

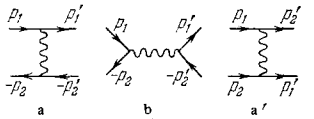

FIG. 7.

Fig. 5a with split horizontal lines and momenta $p_1 = p_1'$ and $p_2 = p_2'$.

The total cross section of these processes diverges because of the presence in the physical region of a photon pole corresponding to Coulomb long-range action. In colliding-beam experiments one therefore usually measures $e^+e^-$ and $e^-e^-$ scattering at large angles close to 90° [29]. The advantage of photon exchange is then lost, since the processes in scattering through finite angles ($\vartheta \sim 1$) decrease with increasing energy. The two diagrams 7a and 7b make equal contributions in the case of large-angle $e^+e^-$ scattering. The $e^+e^-$ scattering cross section is given by [30]

$$d\sigma_{e^+e^-} = 4\pi\alpha^2 \frac{dt}{s^2}\left[\frac{s^2+u^2}{2t^2} + \frac{u^2+t^2}{2s^2} + \frac{u^2}{ts}\right], \qquad (41)$$

where s, t, and u are determined by formula (1). At small t, Eq. (41) goes over into the Rutherford formula (37).

We note that the process $e^-e^-$ or $e^-e^+$ is the only scattering process with a nondecreasing cross section, the amplitude of which is described by the simplest pole diagrams of Fig. 7, and the cross section is accordingly proportional to $\alpha^2$. All other processes with cross section proprotional to $\alpha^2$, namely the $e^-e^+ \to \mu^-\mu^+$ annihilation (Fig. 7b) with muons at the end, the $e^-e^+ \to 2\gamma$ annihilation (Fig. 2c), and also the production of $\rho$, $\omega$, and $\varphi$ resonances and single hadrons (Fig. 7b) are described by pole diagrams which have no photons in the intermediate state of the t-channel. The cross section of these processes decreases with increasing energy. The nondecreasing cross sections of all the remaining processes are proportional to higher powers of $\alpha$.

c) **Bremsstrahlung of one photon.** Bremsstrahlung at high energies in $e^+e^-$ scattering is described by the diagrams of Fig. 8. The amplitude of this process has an additional e, and consequently the cross section has an additional $\alpha = 1/137$ in comparison with $e^+e^-$ scattering. To describe bremsstrahlung in $e^-e^-$ scattering, it is necessary only to reverse the directions of the arrows in the lower electron line of Fig. 8, and to add diagrams with interchanged final electrons.

The circles in the diagrams of Fig. 8 denote that the amplitudes A and B include also diagrams with emission of a photon by the final electron in A and a final positron in B. Only the sum of these diagrams satisfies the gauge-invariance condition (32).

The diagrams for the bremsstrahlung cross section take the form of Fig. 9a and of the diagram symmetrical to it with respect to replacement of $p_1$ by $p_2$ (up by down). These diagrams correspond to the squares of each of the amplitudes—Fig. 8. The cross sections corresponding to the diagrams for the interference of the amplitudes in Fig. 9b decrease with increasing energy, since they have in the t-channel no horizontal photon splittings connected with scattering of virtual particles only. With respect to both pair energies $s_1$ and $s_2$, one of the amplitudes in Fig. 9b contains a photon in the t-channel and is increasing, while the second, which contains no photon in the t-channel, is constant[9]. Diagram 9b for the cross section should therefore be discarded. Let us consider some well-known characteristic features of this process [30-35], which we shall find useful for the understanding of the physics of other processes.

The process in Fig. 9 has three particles in the final state. The encircled block that has no photon in the intermediate state of the t-channel should not be in the asymptotic regime in this case, i.e., all the quantities on which it depends (the energy and the transferred momenta) are of the order of the electron mass m. In the c.m.s., all the particles produced in such a block travel in the same direction, forming angles $\vartheta \sim m/s^{1/2}$ with one another. In our case this means that the produced photon will travel in the direction of travel of the electron or the positron (i.e., forward or backward [29]).

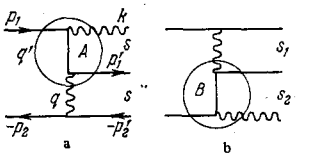


FIG. 8.

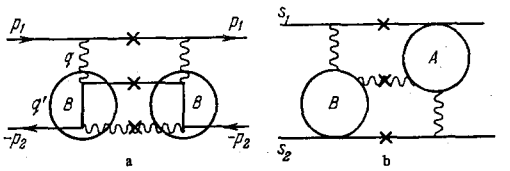


FIG. 9.

To obtain the degree of s in the amplitude, the intermediate photon should have a small momentum $t = q^2 \sim m^2$, i.e., the electrons and positrons should be deflected through angles $\vartheta \sim m/s^{1/2}$ in the scattering.

In the square of the amplitude B of Fig. 9a, after adding the two diagrams, there appears a factor $t/s^2$ (34), the numerator of which cancels out one of the photon propagators in Fig. 9a. As a result, the bremsstrahlung cross section acquires the form (38), where $d\sigma_1$ is the Compton scattering cross section determined by the amplitude B in Fig. 9a. For the Compton scattering, the minimum value of $s_2$ as $t \to 0$ in (39) is

$$s_{2\min} = 2p_2q = 2p_2'k = 2\omega(E_2 - p_2\cos\vartheta)_{\min} = 2\omega(E_2 - p_2) \sim \omega m^2/s^{1/2}. \qquad (42)$$

The range of variation of t in which formula (38) is valid therefore takes the following form in the case of bremsstrahlung:

$$m^6\omega^2/s^3 \leqslant t \ll m^2. \qquad (43)$$

Integration over this region leads to the Weizsacker-Williams logarithm. We emphasize that the Weizsacker-Williams logarithm is a consequence of the zero photon mass. Thus, the main contribution to the bremsstrahlung is made by very small scattering angles of the charged particles, $m^3\omega/s^2 \ll \vartheta \ll m/s^{1/2}$. If we select specially the scattering angles $\vartheta \sim m/s^{1/2}$, then we lose the Weizsacker-Williams logarithm $\ln(s/m^2)$. Finally, if we study scattering through finite angles $\vartheta \sim 1$, then we lose one power: the cross section begins to decrease with increasing energy [29].

The cross section of the process remains constant in the case of emission of photons with $\omega \lesssim s^{1/2}/2$. If photons with $s^{1/2}/2 - \omega \sim m$ are emitted, the cross section is no longer constant and begins to decrease with increasing energy [36]. Photons with $\omega \ll s^{1/2}/2$ correspond in the rest system of the radiating electron ($p_1 = 0$) to infrared photons with energy $\omega' \ll m$. In this region, which is of greatest interest from the experimental point of view, the Compton scattering cross section (41) coincides with the classical Thomson limit $\sigma_0$ as $\omega \to 0$. Replacing the variable $s_2$ (42) by $\omega$ and

taking into account the two diagrams of Fig. 9a corresponding to the emission of an electron and positron (Fig. 8), we obtain the following expression for the bremsstrahlung cross section:

$$d\sigma = 2\sigma^{(0)}(\alpha/\pi)(dt/t)\,d\omega/\omega,\quad \sigma^{(0)} = (8\pi/3)r_0^2,\quad r_0 = \alpha/m. \tag{44}$$

Integrating with respect to dt between the limits of (46), we obtain

$$d\sigma = 16r_0^2\alpha\,[\ln(s/m^2) + (2/3)\ln(m/\omega)]\,d\omega/\omega. \tag{45}$$

Formula (45) is accurate to a constant term. The general asymptotic form of the bremsstrahlung cross section, which is valid for arbitrary $\omega$, is described, accurate to terms of order $m^2/s$, by the formula [33,34]

$$d\sigma = 4r_0^2\alpha\frac{d\omega}{\omega}\frac{\varepsilon-\omega}{\varepsilon}\left(\frac{\varepsilon}{\varepsilon-\omega}+\frac{\varepsilon-\omega}{\varepsilon}-\frac{2}{3}\right)\left[\ln\frac{4\varepsilon^2(\varepsilon-\omega)}{\omega}-\frac{1}{2}\right],\quad \varepsilon = \frac{s^{1/2}}{2}. \tag{46}$$

Integration of the cross section with respect to $\omega$ gives rise to a logarithmic divergence at small $\omega$. The reason for this divergence is that all the processes with charged particles are accompanied by emission of not one but of an infinite number of very soft classical photons, for which perturbation theory (expansion in $\alpha$) does not hold. The lower limit for the frequency of a single photon that can be registered in experiment is determined by the energy resolution of the instrument, which in principle cannot be infinitesimally small. In colliding-beam experiments $\omega_{min} \sim 1$—10 MeV. Formula (46) is meaningful if $\omega \geq \omega_{min}$.

The emission of the classical photon is independent of the fundamental process in our case of elastic scattering, since its frequency $\omega$ is much smaller than all the variables of the main process. Therefore at $\omega \ll t/s^{1/2}$ ($p_1 k \ll t$) the bremsstrahlung cross section can be expressed in the form of the product of the elastic-scattering cross section (41) and the probability da of emission of a classical photon. The expression for da is determined by the square of the classical current, which is equal to the sum of the Feynman diagrams for the radiation emitted by the initial and final particles:

$$da = |M|^2\,d^3k/(2\pi)^3\,2\omega,\quad M = (4\pi\alpha)^{1/2}\,\varepsilon_\mu j_\mu, \tag{47}$$

$$j_\mu = (p_{1\mu}/p_1k) - (p'_{1\mu}/p'_1k). \tag{48}$$

Summation over the photon polarizations $\epsilon_\mu$ leads to the well-known formula for the classical photon emission probability

$$da = (\alpha/2\pi^2)(d\omega/\omega)\,[(p_{1\mu}/p_1n) - (p'_{1\mu}/p'_1n)]^2\,d\Omega_k, \tag{49}$$

where $n_\mu = k_\mu/\omega$. The last factor depends only on the electron mass m and on the momentum transfer $t' = (p'_1 - p_1)^2$, and vanishes as $t' \to 0$[10].

Formula (49) indicates directly the cause of the occurrence of the logarithmic integral with respect to $d\omega$ in (44). We see from (48) that in the case of bremsstrahlung of photons with $\omega \ll s^{1/2}$ the polarizations of the latter have components that are parallel to the momenta $p_1$ and $p'_1$. Photons with $\omega \ll s^{1/2}$, having polarization perpendicular to the momenta $p_1$ and $p'_1$, are not emitted.

The bremsstrahlung mechanism may also govern the production of C-odd vector mesons $\rho$, $\omega$ and $\varphi$ [37], and also of single hadrons [38]. The diagrams for the cross sections of these processes are of the form shown in Fig. 9a, in which the produced bremsstrahlung photon is transformed into a vector meson or a group of hadrons. The cross section for the production of vector mesons in accordance with the mechanism of Fig. 9a is of the order of $10^{-34}$ cm$^2$, and, in analogy with the bremsstrahlung photon, the produced vector meson travels predominantly in the direction of motion of the beams, at angles $\vartheta \sim m_\rho/s^{1/2}$.

The cross section for scattering with emission of two photons in one direction can be obtained by substituting an additional photon in the lower block of Fig. 9a. This cross section is smaller than the cross section for single bremsstrahlung (44) by a factor $\alpha$.

d) **Double bremsstrahlung.** Double bremsstrahlung with the photons moving apart in opposite directions makes it possible to register both protons by the coincidence method. This process is of great interest for experiments with colliding beams, since it is used as a monitor for registration of the collision of beams and for normalization of the cross sections of the investigated processes [35,39]. The cross section of the process is determined by the diagram of Fig. 10, where, as in Fig. 9, the encircled blocks are taken to mean sums of diagrams with a photon emitted by the initial and final electron (positron). At small $t \ll m^2$, the cross section of the process is described by formula (40). Just as in the case of single bremsstrahlung, the encircled blocks containing no photons in the t-channel are not under asymptotic conditions. Consequently, the photons travel at small angles $\vartheta \sim m/s^{1/2}$ to the particles that emit them, which, by virtue of the smallness of $t = q^2 \sim m^2$, are deflected in turn through small angles $\vartheta \sim m/s^{1/2}$. There is no Weizsacker-Williams logarithm for this process, since the square of each block is proportional to t at small values of t, thus cancelling both poles of the photon propagators of Fig. 10. Photons with energies $\omega \ll s^{1/2}/2$ correspond, just as in the case of single bremsstrahlung, to infrared classical photons [35]. Two such photons are emitted independently of each other. There is a correlation between the emission of two hard photons with energy $\omega \sim s^{1/2}$ ($(s^{1/2}/2) - \omega \sim s^{1/2}$), but it is numerically small (<1%). The cross section can therefore be represented approximately as a product of factors, each of which depends on one photon [35,36]

$$d\sigma = (8r_0^2\alpha^2/\pi)\,R(\omega_1)(d\omega_1/\omega_1)\,R(\omega_2)\,d\omega_2/\omega_2, \tag{50}$$

$$R(\omega) = \eta_1^{1/2}[1 - (\omega/E)] + \eta_3^{1/2}(\omega^2/E^2), \tag{51}$$

$$\eta_1 = (5/4) + (7/8)\,\zeta(3),\quad \eta_3 = (7/8)\,\zeta(3) = 1.052. \tag{52}$$

This multiplicative property was observed experimentally [29].

The double bremsstrahlung mechanism can also govern the production of one or two C-odd vector mesons $\rho$, $\omega$, and $\varphi$. In this case, one or both bremsstrahlung photons of Fig. 10 are transformed into vector mesons. The cross section for the production of a vector meson and a photon emitted in opposite directions along the direction of beam motion should be of the order of $10^{-35}$—$10^{-36}$ cm$^2$.

e) **Scattering with production of charged pairs.** The next process is the process of production of the pair $e^+e^-$ or $\mu^+\mu^-$ [12]. The cross section of this process is described by the diagram of Fig. 11. The circle around the central block 3 denotes, as before, that it is necessary to take a sum of diagrams with interchanged photon lines.

A power-law constancy of the cross section of this process is obtained if the central block 3 with electrons in the intermediate state in the t channel is not in the

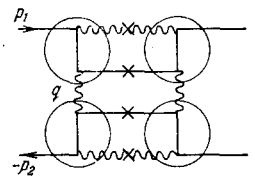


FIG. 10.

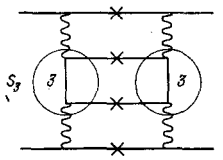


FIG. 11.

asymptotic region $s_3 \sim m^2$. The cross section diagram in Fig. 11 has two successive photon splittings in the t-channel, which leads to the appearance of one large logarithm $\ln(s/m^2)$. In addition, the amplitude of Fig. 11 has two Weizsacker-Williams logarithms, one for each of the intermediate amplitude photons, since the square of the block 3 is proportional to the product $t_1t_2$ as $t_1, t_2 \to 0$. These logarithms, as already explained, are due to very small scattering angles $\vartheta \ll m/s^{1/2}$ of the beam particles. They vanish if the scattering angles are $\vartheta \lesssim m/s^{1/2}$. Thus, the total cross section for $e^+e^-$ pair production is proportional to $\ln^3(s/m^2)$ in the principal logarithmic approximation. The general expression for the total cross section, accurate to terms $\sim m^2/s$, is[40,41]

$$\sigma_{4l} = (28\alpha^2/27\pi)\, r_0^2\, [\rho^3 - 6.35\rho^2 - 11.35\rho + 100], \quad \rho = \ln(s/m_e^2). \quad (53)$$

The last two terms in the square brackets are due both to the diagrams of Fig. 11 and to diagrams in which one of the outermost (upper or lower) blocks with photons in the intermediate state of the t-channel, together with the electron block 3 (virtual Compton effect), is replaced by cross-section diagrams in which one or both amplitudes do not contain photons in the t-channel. The contribution of the last three terms in the square brackets of (53) ranges from 40 to 20% at energies $s^{1/2}$ from 1 to 1000 GeV.

The maximum value of the cross section ($\sim \ln^3(s/m^2)$) is obtained when the produced pair travels in the direction of the beams with large velocities and small relative angles. The production of such a pair is very difficult to register. In experiments one usually registers charged pairs with high energy, traveling at large angles relative to the beams and relative to each other[29]. The energy invariant $s_3$ of block 3 is in this case large, $s_3 \sim s$, and the dependence on the mass m drops out in this block. With such a kinematics, the cross section no longer has power-law constancy, but decreases like $1/s_3$. The regions of integration with respect to the Weizsacker-Williams variables $t_1$ and $t_2$ (39) are transformed into

$$m^2 \ll t_i \ll s_3 \sim s, \quad (54)$$

and integration over these regions leads as before to two large logarithms ($\ln^2(s_3/m^2)$)[40,42]. The third energy logarithm is transformed into $\ln(s/s_3)$ and becomes of the order of unity. The condition (54) corresponds to the following angle between the scattered particles

$$m/s^{1/2} \ll \vartheta_i \ll 1. \quad (55)$$

A value $\sim 10^{-31}$ cm$^2$ was registered in Novosibirsk[29] for the cross section of pair production in the indicated kinematics.

In addition to an electron pair, a muon pair can also be produced. The cross section for the production of this pair is given by (53), in which $r_0 = e/m_e$ should be substituted by $r_0 = e/m_\mu$, where $m_\mu$ is the muon mass. The first two terms in the square brackets of (53), which contain $\rho^3$ and $\rho^2$, coincide with the case of electron-pair production. The last two terms, however, become $-290\rho + 2000$[40,41]. Such large values of these terms significantly alter the contribution of the first two terms. At an energy $s^{1/2} \sim 10$ GeV, the summary contribution of the square brackets is one-fourth of the contribution of the first two terms. At energies $s^{1/2} \sim 1$ GeV, the muon-pair production cross section calculated from formula (53) is negative[40] and this formula cannot be used (the terms $\sim m^2/s$ should cancel out this negative quantity).

The electron-positron pair in Fig. 11 can be produced in the bound state, positronium. The cross section for positronium production also contains three logarithms, but the phase volume of block 3 is smaller by a factor $\alpha^3$ than the phase volume of the free pair, since the average relative momentum of the particles and of the positronium is equal to $\bar{p}_{pos} = m\alpha$, and consequently $\bar{p}_{pos}^3/p^3 \sim m^3\alpha^3/m^3 \sim \alpha^3$. This cross section is of the order of $10^{-33}$ cm$^2$ at $s^{1/2} = 7$ GeV[43].

All the listed processes described by Fig. 11 can be accompanied by simultaneous emission of one or several bremsstrahlung photons. The cross section with emission of one photon is obtained when a real photon is substituted in block 3 (the upper and lower electron lines) in Fig. 11 and contains three (two) logarithms. The cross section for pair production with emission of two photons in opposite directions along the beams is determined by diagrams of the type of Fig. 11 with two photons substituted in the two outermost electron lines, and contains only one logarithm.

The diagram of Fig. 11 can be generalized to the case of production of two or more charged particle pairs (Fig. 12)[44,45]. The diagram for the production of two pairs contains three blocks in the asymptotic regime with photons in the t-channel, which yields two energy logarithms. Together with the two Weizsacker-Williams logarithms (for each pair of outermost photons), this cross section thus contains $\ln^4(s/m^2)$. At $s^{1/2} = 7$ GeV, the total cross section for the production of two $e^+e^-$ pairs turns out to be of the order of $10^{-31}$ cm$^2$[44,45].

In the diagrams of the type of Fig. 12, each produced pair gives rise to a small quantity of the order of $\alpha^2\ln(s/m^2)$. It is possible to sum the sequence in Fig. 12 with an arbitrary number of produced pairs[8,9]. Since each n-th term of the sequence is positive and has a logarithmic growth of the power $[\alpha^2\ln(s/m^2)]^{n+1}$, the sum has at fantastically high energies a power-law growth with an exponent equal to $(11/32)\alpha^2$.[8,9]

The mechanism of Fig. 11 can result in the production of individual C-odd hadrons[46], resonances[47] and hadron groups[42,48]. The cross section for the production of individual hadrons or resonances contains three logarithms, like the positronium production cross sec-

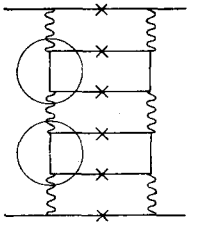

FIG. 12.

tion, and is of the order of $10^{-33}$—$10^{-34}$ cm$^2$ at $s^{1/2} \sim 7$ GeV. The cross section for the production of the group of hadrons is obtained by replacing the block 3 of Fig. 11 with a hadron block. If it is assumed that the production of a group of hadrons by two photons (block 3) has a constant cross section, then block 3 must be taken in the asymptotic regime at $s_3 \gg m^2$. A constant cross section can be obtained by assuming that block 3 has a unity-spin particle (vacuum pole) in the intermediate state of the t-channel (at small t). In this case all the blocks of Fig. 11 are in the asymptotic regime. Taking into account two Weizsacker-Williams logarithms, we find that the cross section for the production of a group of hadrons, like the production cross section of two pairs in Fig. 12, is proportional to $\ln^4(s/m^2)$ (two of these logarithms, which appear after integration with respect to the energy variables (see (17)) contain the ratio of s to the hadron masses). In the case of hadron production, $r_0^2 = \alpha^2/m_e^2$ in (53) is replaced by $\alpha^3/m_\pi^2$. Since $\alpha \sim m_e/m_\pi$ approximately, the cross sections for the production of two electron-positron pairs and a group of hadrons turn out to be of the same order. Detailed estimates[48] for the total hadron-production cross section yield $\sigma \sim 10^{-32}$ cm$^2$ at $s^{1/2} \sim 7$ GeV.

## 4. PROCESSES WITH CROSS SECTIONS THAT DECREASE WITH INCREASING ENERGY

a) **Doubly logarithmic asymptotic expressions.** We have seen that all the large-angle scattering processes have cross sections that decrease with increasing energy. Decreasing cross sections are possessed also by small-angle scattering processes that have no photons in intermediate states of the t-channel, and also processes of scattering through angles close to 180° ($u \sim m^2$).

For all these processes, the radiative corrections connected with the emission of both virtual and real photons, which are small in the case of processes with constant cross section, contain a maximum possible number of logarithms of s. For each photon line, i.e., for each power of $\alpha$, we obtain $\ln^2(s/m^2)$. The parameter of the perturbation-theory series becomes $(\alpha/\pi)\ln^2(s/m^2)$ and is not small ($(\alpha/\pi)\ln^2(s/m^2) \sim 1$ at $s^{1/2} \sim 10$ GeV). It thus becomes necessary to sum all perturbation-theory terms containing this parameter, which are called doubly logarithmic (DL) terms. At $(\alpha/\pi)\ln^2(s/m^2) \gtrsim 1$ and $(\alpha/\pi)\ln(s/m^2) \ll 1$, summation of the sequence of DL terms gives for the entire amplitude a correct asymptotic formula that holds true up to very high energies ($(\alpha/\pi)\ln(s/m^2) \sim 1$ at $s^{1/2} \sim 10^{100}$ GeV). The radiative correction, which contains singly-logarithmic terms, can be taken into account by using perturbation theory.

An important feature of the DL approximation is that any complicated Feynman diagram makes a DL contribution only if any arbitrary internal block of this diagram is in the asymptotic regime and contains a DL contribution with respect to its external variables. If this is not the case and some block is not contained in the asymptotic expression or has no DL contribution, then it contains a definite number of powers of the small parameter $\alpha$, which is not cancellable by the squares of the large logarithms. It is therefore sufficient to seek the simplest Feynman diagrams containing DL contributions. In particular, one can immediately discard all the diagrams that include closed charged loops, since the latter contain no DL contributions.

To find the DL Feynman diagrams, we divide all photons into two groups, depending on their polarization with respect to the initial-particle momenta $p_1$ and $p_2$ making up the large variable s (1). We resolve the polarizations of all the real and virtual photons into longitudinal and transverse parts[13,14]:

$$\gamma_\mu = \gamma_\mu^{\parallel} + \gamma_\mu^{\perp}, \quad \gamma_\mu^{\parallel}\hat{p}_i + \hat{p}_i\gamma_\mu^{\parallel} = 2p_{i\mu}, \quad \gamma_\mu^{\perp}\hat{p}_i + \hat{p}_i\gamma_\mu^{\perp} = 0. \tag{56}$$

The photons having parallel polarization will be called "bremsstrahlung photons" and designated by dashed lines (Fig. 13). It is precisely these photons which contribute to the amplitude of the accompanying bremsstrahlung (49). Photons with perpendicular polarization will be called "ladder" photons and denoted by wavy lines (see Fig. 13).

The convenience of division into bremsstrahlung and ladder photons lies in the fact that these two types of photons give DL contributions in opposite situations, in that a virtual or real bremsstrahlung photon makes a DL contribution only if it joins charged lines of the amplitude diagram or cross sections with large momentum transfer. Ladder photons, to the contrary, make a DL contribution only if they join charged lines with small momentum transfer.

Let us consider, for example, diagrams of two-particle processes (Fig. 13), under the condition that (see (1))

$$s \gg m^2, \quad t \ll s, \quad u \sim s. \tag{57}$$

It is easy to see that under condition (57), only one of the diagrams 13a and 13b, in which one photon joins electron lines with small momentum transfer t, survives, namely the diagram (a) with the ladder photon. Indeed, in the c.m.s., for example, the parallel components of the bremsstrahlung-photon polarization $\gamma_\mu^{\parallel}$ can be expressed in the form

$$\gamma_0 = (\hat{p}_1 + \hat{p}_2)/s^{1/2}, \quad \gamma_3 = (\hat{p}_1 - \hat{p}_2)/s^{1/2}. \tag{58}$$

The charged spinor ends of the diagrams of Fig. 13 correspond to the Dirac bispinors $u_p$ (9). Taking the Dirac equation $\hat{p}u_p = mu_p$ into account, we find that diagram 13b with the bremsstrahlung photon is of the order $m^2/s$ relative to the diagram 13a with the ladder photon, which contains the polarizations $\gamma_\mu^{\perp}$ ($\gamma_1$ and $\gamma_2$ in the c.m.s.)[11].

Principal among the diagrams 13c—13f will be diagrams (c) and (d), in which the bremsstrahlung photons join lines with large momentum transfer. Transferring the momenta $\hat{p}_1$ and $\hat{p}_2$ in the spinor numerators of these diagrams towards the corresponding free ends, we obtain from the commutation of $\hat{p}_1$ and $\hat{p}_2$ with $\gamma_\mu$ the value $4p_1p_2 = 2s$ for diagrams 13c and 13d, and a value on the order of the correction $m^2$ for the diagrams 13e and 13f. Thus, in the presence of a large momentum transfer, the emission of a bremsstrahlung photon is always favored rather than that of a ladder photon. In the diagrams 13g and 13h, the bremsstrahlung photon makes a smaller contribution than the ladder photon, for the same reason

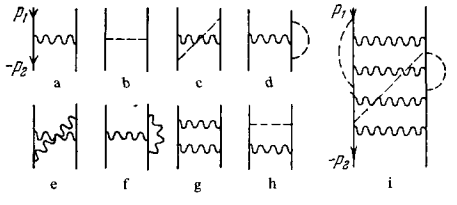


FIG. 13.

as in diagrams 13a and 13b. In diagrams 13g with two parallel ladder photons, the DL contribution is the consequence of cancellation of one spinor denominator by two spinor numerators[3,14].

Summarizing the foregoing, we can state that all the DL diagrams take the form of ladder diagrams with ladder photons as the rungs, in which bremsstrahlung photons are inserted in arbitrary manner in such a way that the latter join charged lines with large momentum transfer (diagram 13i).

b) **Poisson distribution of bremsstrahlung.** In the diagrams containing bremsstrahlung photons (Fig. 13c, d, i) it is convenient to choose as the integration variables the bremsstrahlung-photon momenta k rather than the variables q (Fig. 14). For a real bremsstrahlung photon it is necessary to replace the bremsstrahlung-photon propagator by $\delta(k^2-\lambda^2)$. The photon mass $\lambda$ has been introduced to eliminate the infrared divergence. The square of the logarithm in the bremsstrahlung is seen directly from formula (49). At large $t \sim s$, the integration of the latter factor over the angles yields $\ln(t/m^2)$. The second logarithm stems from the integration with respect to $d\omega$.

It is convenient to calculate the integral (47) over the phase volume in terms of the invariant variables (12):

$$k=p_1\beta-p_1'\alpha+k_\perp, \quad t\approx 2p_1\cdot p_1'\gg m^2, \tag{59}$$

$$2p_1k=t\alpha+2m^2\beta, \quad 2p_1'k=t\beta+2m^2\alpha. \tag{60}$$

Eliminating $\delta(k^2-\lambda^2)$ (10) by integrating with respect to $d^2k_\perp$ (14) and separating only the DL contribution, we obtain for (47)

$$a=(\alpha/\pi)\int_\lambda^t(t\alpha)^{-1}\,dt\alpha\int(t\beta)^{-1}\,dt\beta=(\alpha/\pi)\int d\xi\int d\eta \tag{61}$$

under the condition

$$\begin{aligned} &t\gg t\alpha\gg m^2\beta,\\ &t\gg t\beta\gg m^2\alpha, \end{aligned} \qquad -k_\perp^2=t\alpha\beta\gg\lambda^2,$$

or

$$\begin{aligned} &\rho>\xi>\eta-\rho,\\ &\rho>\eta>\xi-\rho, \end{aligned} \qquad \xi+\eta-\rho\equiv\zeta>-L, \tag{62}$$

where

$$\begin{aligned} &\xi=\ln(t\alpha/m^2), \quad \eta=\ln(t\beta/m^2), \quad \rho=\ln(t/m^2),\\ &L=-\ln(\lambda^2/m^2), \quad \zeta=\ln(-k_\perp^2/m^2). \end{aligned} \tag{63}$$

Calculation of the integral (61) within the limits (62) is best carried out graphically[14,19] (see Fig. 14). In terms of the logarithmic variables, the integral (61) is equal to the area of the circumscribed figure, or $\rho L + (\rho^2/2)$. This contribution is produced if the emission of bremsstrahlung photons is not limited experimentally; it coincides with the contribution of the virtual bremsstrahlung photons[12]. The DL contribution of the bremsstrahlung photon vanishes at lower momentum transfer between the electron lines with momenta $p_1$ and $p_1'$ ($t \sim m^2$).

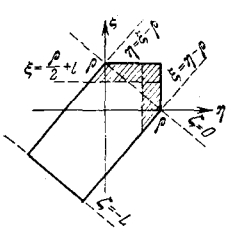

FIG. 14.

1) As seen from Fig. 14, the DL contribution stems both from large $-k_\perp^2 \gg m^2$ ($\zeta > 0$) and from small $-k_\perp^2 \ll m^2$ ($\zeta < 0$). The contribution from the small $k_\perp$ is connected with the zero photon mass and vanishes at $\lambda^2 \sim m^2$ ($L = 0$). In spite of so close a connection with the infrared divergences, the DL contribution from small $k_\perp$ of the bremsstrahlung photons is contained not only in diagrams with infrared divergence (see, e.g., Fig. 13i). However, the summary DL contribution of all diagrams has the classical property of Poisson distribution, just as the contribution of the infrared photons[50,51], namely, the DL contribution connected with small $-k_\perp^2 \ll m^2$ of real and virtual photons is separated in the form of a Poisson factor for arbitrary processes, including processes with participation of hadrons accompanied by large momentum transfer between two charged particles:

$$d\sigma_n = d\sigma^{(0)}\,(a^n/n!)\,e^{-a}, \tag{64}$$

$$a=(\alpha/\pi)\,\rho L. \tag{65}$$

where $a^n/n!$ is the contribution of n real photons and $e^{-\alpha}$ is the contribution of the virtual photons. The probability of emission of a bremsstrahlung photon a with $k_\perp^2 \ll m^2$ is equal to the area of the circumscribed figure to the left of the line $\zeta = 0$ on Fig. 14; $d\sigma^{(0)}$ is the cross section of the main process and contains no DL contribution from virtual bremsstrahlung photons with $-k_\perp^2 \ll m^2$; $d\sigma^{(0)}$ contains, generally speaking, a contribution from bremsstrahlung photons with $-k_\perp^2 \gg m^2$.

It is seen directly from (64) that as $\lambda \to 0$ the cross section with production of a finite number of photons with $k_\perp^2 \ll m^2$ vanishes, and consequently such processes cannot be registered. If an infinite number of bremsstrahlung photons with $-k_\perp^2 \ll m^2$ is emitted, the Poisson factor becomes equal to unity and the cross section coincides with $d\sigma_0$. We shall assume below that all the processes are accompanied by emission of an infinite number of bremsstrahlung photons bounded by the condition $-k_\perp^2 \ll m^2$ ($\zeta < 0$), and investigate only the contribution of bremsstrahlung photons[13] with $-k_\perp^2 \gg m^2$ ($\zeta > 0$), which do not depend on the photon mass $\lambda$.

In the case when the investigated real bremsstrahlung photons with small $-k_\perp^2 \ll m^2$ are experimentally limited by additional conditions, the cross section of the process must be additionally multiplied by an exponential whose argument is equal to the difference between the contributions of the real and virtual bremsstrahlung photons. If the experimental limitations are specified, this argument can easily be obtained from Fig. 14. Particular cases of such a situation will be considered below. We now proceed to consider concrete processes containing DL contributions.

2) Bremsstrahlung in large-angle scattering, when the direction of travel of the charges changes radically, is doubly logarithmic. In this case there is a large momentum transfer between all the charged lines, and there are no ladder-photon contributions. Bremsstrahlung photons, on the other hand, contribute when any pair of charged lines is joined. Thus, at large energies and scattering angles (when $s \sim |t| \sim |u| \gg m^2$) the dependence on the electron mass m drops out, and the bremsstrahlung photons can be regarded as classical (infrared) and exerting no influence on the main process, if the condition $\omega \ll s^{1/2}$ or $p_1k$, $p_2k \ll s$ is satisfied (in

place of the condition $\omega \ll m$, $p_1k$, $p_2k \ll m^2$ at finite energies). Since all the logarithms come from precisely these regions (the regions $p_ik \sim s$ and $k_\perp^2 \sim s$ produce no logarithm), the entire DL contribution of the bremsstrahlung comes from classical photons[16-18]. Classical bremsstrahlung photons are radiated independently of one another and of the main process. The sum of their contribution is determined by the Poisson factor (64), where $d\sigma^{(0)}$ does not contain a contribution of bremsstrahlung photons and describes the cross section of the main process in the Born approximation[14]. The quantity a in (64) is equal to the total area of the circumscribed figure in Fig. 14, multiplied by the number r of the charged lines of the process:

$$a = r(\alpha/2\pi)(\rho^2 + 2\rho L), \quad L = -\ln(\lambda^2/m^2), \quad \rho = \ln(s/m^2); \qquad (66)$$

r = 1 for the processes $e^+e^- \to 2\gamma$, $3\gamma$ and r = 2 for $e^+e^- \to e^+e^-$ and $e^+e^- \to \mu^+\mu^-$.[15]

If the emission of real photons is not registered experimentally, then the sum over n in (64) gives unity and the cross section coincides with $d\sigma^{(0)}$. In the case when an infinite number of real photons with $-k_\perp^2 \ll m^2$ is emitted and emission of n photons with $-k_\perp^2 \gg m^2$ is registered, it is necessary to subtract from a (66) the contribution of the photons with $-k_\perp^2 \ll m^2$; the cross section of such a process is described by formula (64) with the quantity a determined by formula (66) at L = 0.

In most experiments, however, one fixes the emission of the photons with $\omega \geq \omega_{min}$[29]. An elastic event is assumed to be an event in the absence of photon emission with $\omega \geq \omega_{min}$. In this case it is necessary to subtract from a (66) the contribution of photons with $\omega \leq \omega_{min}$, which can easily be obtained with the aid of Fig. 14. At $\omega \lesssim \omega_{min}$ we have

$$\omega = k_0 = p_{10}\beta - p_{20}\alpha = (s^{1/2}/2)(\beta - \alpha) \leqslant \omega_{min} < s^{1/2},$$

or $\xi < (\rho/2) + l$, $\eta < (\rho/2) + l$, $l = \ln(2\omega_{min}/m) < \rho/2$. As a result we get

$$\Delta = a - a|_{\omega<\omega_{min}} = r(\alpha/2\pi)(\rho^2 - 2l\rho). \qquad (67)$$

Thus, the cross section of the process in which a fixed number n of photons with $\omega \geq \omega_{min}$ is emitted is given by formula (64) in which a is replaced by $\Delta$ (67) (L is replaced by $-l$). Since we have discarded the single-logarithm terms, expression (67) is valid under the condition $(\rho/2) - l \gg 1$. At $\omega_{min} \sim s^{1/2}/2$, there is no DL contribution of the bremsstrahlung.

We note that the same formula is also valid for a fixed energy $\epsilon$ lost by the electron to radiation. It is merely necessary to replace $\omega_{min}$ by $\epsilon$. However, no measurements of the final-electron energies have as yet been made in colliding-beam experiments.

Another way of limiting real bremsstrahlung is to impose limitations on the noncollinearity angle of the elastic process. The expression (67) for $\Delta$ can in this case likewise be easily obtained with the aid of the diagram of Fig. 14. The DL contribution of the bremsstrahlung is significant only if the noncollinearity angle is small, $1 \gg \Delta\vartheta \gtrsim m/s^{1/2}$. In modern colliding beams we have $\Delta\vartheta \sim 1^\circ$, and then the DL contribution of the bremsstrahlung photons is almost entirely cancelled and becomes comparable with the singly-logarithmic contribution[29].

c) Multiphoton annihilation. 1) We now consider the process of multiquantum annihilation of an $e^+e^-$ pair[53]. This process is described by a diagram of the type shown in Fig. 15 at t = 0 ($p_1 = p_1'$, $p_2 = p_2'$) with replacement of all the propagators of both the bremsstrahlung and the ladder photon lines joining two electron lines by $\delta$ functions (10) with positive energy. In the presence of ladder photons, the dL contribution of the bremsstrahlung photons with $-k_\perp^2 \gg m^2$ depends on the ladder variables at the points of emission and absorption of the bremsstrahlung photon. If the emission and absorption points are fixed, however, the bremsstrahlung photons are emitted independently of one another and have a Poisson distribution[54]. When calculating the total cross section for the annihilation into an arbitrary number of photons, i.e., in the absence of limitations on the bremsstrahlung photons, the contributions of the real and virtual bremsstrahlung photons cancel each other, just as in the case of (64). In diagram language this is expressed in the fact that at fixed photon emission and absorption points each group of virtual photons joining one and the same charged line corresponds to a group of real photons joining different charged lines, with each photon making a contribution of opposite sign.

As a result, the contribution of the bremsstrahlung photons cancels out and the total cross section of multiquantum annihilation is determined only by the sequence of the ladder diagrams of Fig. 15 for the cross section.

To calculate the contribution of the ladder diagrams of Fig. 15, we use the Sudakov variables and the ready-made expression (21) for the phase volume. The two amplitudes forming the ladder of Fig. 15 depend only on the electron propagators $(\hat{q}_i + m)/(q_i^2 - m^2)$, the square of which at large $t_i$

$$s \gg t_i = q_i^2 \gg m^2, \qquad (68)$$

is proportional to $1/t_i$.

The spinor structure of the numerators of the ladder can easily be obtained under the condition (68). Let us examine the first diagram of the ladder type in Fig. 13g, corresponding to annihilation into two ladder photons and into an arbitrary number of bremsstrahlung photons.

Under condition (68), the spin structure of the numerators can be expressed in the form

$$\gamma_{\mu_2}^\perp \hat{q}\gamma_{\mu_1}^\perp \cdot \gamma_{\mu_1}^\perp \hat{q}\gamma_{\mu_2}^\perp, \quad \hat{q} = \gamma_\mu q_\mu. \qquad (69)$$

In (69), the Dirac spinors $u_{p_i}$ have been omitted, and the center dot separates the numerators of two spinor lines. The parallel component of the vector q, which is equal to $p_1\beta - p_2\alpha$, yields after commutation with $\gamma_\mu^\perp$ and application of the Dirac equation $\hat{p}_i u_{p_i} = m u_{p_i}$, a small quantity of the order of $\alpha$, $\beta \ll 1$ (16) (which is equivalent to the loss of two logarithms). The remaining perpendicular components of the vector q should be taken with equal projections in both electron lines (69), in order that the resultant squares of the components $q_i^2$

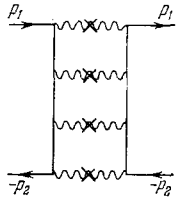

FIG. 15.

can cancel out one spinor denominator. Averaging over the angle $\varphi$ in the perpendicular plane and using the equality

$$\overline{q_1^2} = q_\perp^2 \overline{\cos^2\varphi} = \overline{q_2^2} = q_\perp^2 \overline{\sin^2\varphi} = q_\perp^2/2, \tag{70}$$

we obtain the following expression for the numerator (69):

$$\gamma_{\mu_2}^\perp \hat{q}\gamma_{\mu_1}^\perp \cdot \gamma_{\mu_1}^\perp \hat{q}\gamma_{\mu_2}^\perp = (1/2)\, q_\perp^2 \gamma_{\mu_2}^\perp \gamma_\sigma^\perp \gamma_{\mu_1}^\perp \cdot \gamma_{\mu_1}^\perp \gamma_\sigma^\perp \gamma_{\mu_2}^\perp = 2q_\perp^2 \gamma_{\mu_1}^\perp \cdot \gamma_{\mu_2}^\perp, \tag{71}$$

where all the indices of the $\gamma$ matrices run through only two values, 1 and 2, corresponding to the perpendicular plane in the c.m.s. Thus, we see that the spinor structure of the square in Fig. 13g leads to the spinor structure of the simplest pole diagram. By adding one more rung to Fig. 13g and performing similar transformations with the numerator, we obtain

$$\gamma_{\mu_3}^\perp \hat{q}_2 \gamma_{\mu_2}^\perp \hat{q}_1 \gamma_{\mu_1}^\perp \cdot \gamma_{\mu_1}^\perp \hat{q}_1 \gamma_{\mu_2}^\perp \hat{q}_2 \gamma_{\mu_3}^\perp = 2q_{1\perp}^2 2q_{2\perp}^2 \gamma_{\mu_1}^\perp \cdot \gamma_{\mu_1}^\perp \tag{72}$$

etc. If, furthermore, we take (18) and (68) into account, we can express the product of the ladder amplitudes contained in the diagram for the cross section with n rungs in Fig. 15 in the form

$$|M^n|^2 = 4\pi\alpha \gamma_\mu^\perp \cdot \gamma_\mu^\perp \prod_{i=1}^{n-1} (2/t_i)\, \vartheta(t_i - m^2) \tag{73}$$

Substituting (73) and (17) in (5), using the recurrence relations (21), (22), and (23), and integrating over all the invariants, we find that the contribution to the cross section of the ladder diagram with n rungs $\sigma_n = (2s)^{-1}|M^n|^2 d\Gamma_n$ satisfies the recurrence relation

$$\sigma_n = \sigma_n(s, m^2), \tag{74}$$

$$\sigma_n(s\beta, t) = (s\beta)^{-1}(\alpha/2\pi) \int (t')^{-1}\, dt' \int ds\beta' \sigma_{n-1}(s\beta', t'), \tag{75}$$

$$t'/s\beta' \gg t/s\beta, \quad s\beta \gg s\beta', \quad t' \gg m^2, \tag{76}$$

$$\sigma_1(s\beta, t) = \pi \bar{f}_0 \delta(s\beta - t), \tag{77}$$

$$f_0 = (4\pi\alpha/s)\, \gamma_\mu^\perp \cdot \gamma_\mu^\perp, \quad \bar{f}_0 = 4\pi\alpha\, \mathrm{Sp}\,(\hat{p}_2 \gamma_{\mu_\perp} \hat{p}_1 \gamma_{\mu_\perp})/4s = 4\pi\alpha, \tag{78}$$

where $f_0$ in (78) is the contribution of the pole diagram 13a, and the bar over $f_0$, i.e., $\bar{f}_0$ in (78) and (77), denotes averaging over the initial polarizations of the electrons and positrons.

The expression for $\sigma_1$ in (77) is the imaginary part of the pole diagram of Fig. 13a, and vanishes at $s\beta = s$ and $t = m^2$, meaning that an electron-positron pair cannot be converted into a real photon. The total cross section is equal to the sum of the terms (74) from n = 2 to infinity. However, by virtue of the vanishing of (77) for real particles, the summation can be carried out from n = 1. Summing both sides of (75) over n from n = 1, we obtain

$$\sigma_{\infty\gamma} = \sum_{n=1}^{\infty} \sigma_n = \sigma(s, m^2), \tag{79}$$

$$\sigma(s\beta, t) = \sigma_1(s\beta, t) + (s\beta)^{-1}(\alpha/2\pi) \int (t')^{-1}\, dt' \int ds\beta' \sigma(s\beta', t'), \tag{80}$$

where $\sigma_1$ is defined in (77) and the conditions (76) are satisfied. To solve Eq. (80) it is convenient to change over to the logarithmic variables

$$\rho = \ln(s/m^2), \quad \xi = \ln(t/s\beta) + \rho, \quad \eta = \rho - \ln s\beta, \tag{81}$$

$$(s\beta = s,\ t = m^2) \to (\xi = \eta = 0). \tag{82}$$

Multiplying (80) by $s\beta$, recognizing that

$$s\beta\delta(t - s\beta) = \delta(\rho - \xi),$$

and introducing the new function

$$s\beta\sigma(s\beta, t) = \pi \bar{f}_0 (\partial/\partial\rho)\, \vartheta(\rho - \xi)\, A(\rho; \xi, \eta), \tag{83}$$

we obtain for $A(\rho; \xi, \eta)$ an equation of the type

$$A(\rho; \xi, \eta) = 1 + (\alpha/2\pi) \int_\xi^\rho d\xi_1 \int_\eta^{\xi_1} d\eta_1 A(\rho; \xi_1, \eta_1). \tag{84}$$

Solution of this equation[3] [16)] yields

$$A(\rho, 0, 0) = (2/x) I_1(x), \quad x^2 = (2\alpha/\pi)\rho^2, \tag{85}$$

where $I_1(x)$ is a Bessel function of imaginary argument.

With the aid of (85), (83), and (79) we obtain

$$\sigma_{\infty\gamma} = s^{-1} \bar{f}_0 \pi (\partial/\partial\rho)(2/x) I_1(x). \tag{86}$$

after calculating the derivative in (86) we obtain ultimately[53]

$$\sigma_{\infty\gamma} = \sigma_{2\gamma}^0 [(8/x^2) I_2(x)]; \quad x^2 = (2\alpha/\pi)\rho^2, \quad \rho = \ln(s/m^2), \tag{87}$$

$$\sigma_{2\gamma}^{(0)} = (2\pi\alpha^2/s)\rho, \quad (8/x^2) I_2(x) = 1 + (x^2/12) + \ldots + [x^{2n}/n!(2+n)!\, 2^{2n-1}], \tag{88}$$

where $\sigma_{2\gamma}^{(0)}$ is the cross section of two-quantum annihilation in the Born approximation. The n-th power of the expansion (88) has the meaning of the cross section for annihilation into n + 2 ladder quanta, accompanied by emission of an arbitrary number of bremsstrahlung photons.

With logarithmic accuracy, we can write for the function that depends only on ln s,

$$\mathrm{Im}\, F(\rho) = (2i)^{-1}[F(\ln(s/m^2)) - F(\ln(-s/m^2))] = \pi(\partial/\partial\rho) F(\rho), \tag{89}$$

Therefore

$$\sigma_{\infty\gamma} = s^{-1}\, \mathrm{Im}\, \overline{F(\rho, 0)}, \quad F(\rho, 0) = f_0 (2/x) I_1(x). \tag{90}$$

Equation (90) is the optical-theorem expression, where the amplitude $F(\rho, 0)$ is the amplitude of the ladder diagram of Fig. 15, in which all $\delta$ functions of the photon lines are replaced by ordinary photon propagators. Since $\sigma_{\infty\gamma}$ (86) is the total cross section for annihilation into an arbitrary number of photons without allowance for the production of electron-positron pairs at the end, it follows that $F(\rho, 0)$ does not coincide with the elastic-scattering amplitude. The main contribution to the elastic-scattering amplitude is made by the diagrams of Figs. 9—12, which contain photons in the intermediate state of the t-channel, and are s times larger than the amplitude (90), which has no photons in the t-channel. The imaginary parts of the diagrams in Figs. 9—12 in the t-channel correspond to cross sections with electron-positron pairs in the final state.

If we add the cross sections with different numbers of bremsstrahlung and ladder photons at a fixed total number of photons, we can obtain the cross section for annihilation into a specified number of unpolarized photons. The Born approximation of two-quantum annihilation coincides in the DL approximation with the cross section for annihilation into two ladder quanta, accompanied by emission of an infinite number of bremsstrahlung photons. The cross section of the true two-quantum annihilation with emission of two ladder photons and without emission of bremsstrahlung photons with $-k_\perp^2 \gg m^2$ is described by the s-channel imaginary part of

the diagram of Fig. 13g, with an arbitrary number of virtual bremsstrahlung photons joining parts of one and the same electron line[17], and takes the form [3]

$$\sigma_{2\gamma}=\sigma_{2\gamma}^{(0)}\exp(-\alpha\rho^2/2\pi)\int_0^\rho \exp(\alpha y^2/2\pi)\,dy,$$
$$\sigma_{2\gamma}^{(0)}=2\pi\alpha^2\rho/s \qquad (91)$$

We present also the cross section for annihilation into three unpolarized photons, one of which can be a bremsstrahlung photon with $-k_\perp^2 \gg m^2$ [53]:

$$\sigma_{3\gamma}=\frac{2\alpha^3}{s}\int_0^\rho d\zeta\exp\left[-\frac{\alpha}{\pi}\left(\zeta\rho-\frac{\zeta^2}{2}\right)\right]\left[\rho\zeta-\frac{\zeta^2}{2}+\frac{\pi}{\alpha}\int_0^\zeta\frac{dx}{x}\left\{\exp\left[\frac{\alpha}{\pi}(\rho-\zeta)x\right]-1\right\}\right],$$
$$\sigma_{3\gamma}^{(0)}=\frac{\alpha^3}{s}\rho^3. \qquad (92)$$

Formula (91), as well as (92), is valid in the case when an infinite number of bremsstrahlung photons with $-k_\perp^2 \ll m^2$ is emitted[18].

All the DL terms in the considered formula come from the region of large $t_i$ satisfying the inequality (68). Such values of $t_i$ correspond to the following photon scattering angles $\vartheta$:

$$1 \gg \vartheta \gg m/s^{1/2}. \qquad (93)$$

If we fix the photon-scattering angles near the upper or lower limit of (93), then the DL terms vanish and the cross section for multiquantum annihilation coincides in the DL approximation with the two-quantum cross section. Two-quantum annihilation at large angles $\vartheta \sim \pi/2$ has been measured thus far in colliding beams.[29]

Thus, to measure the DL cross section of multiquantum annihilation it is absolutely necessary to cover the angle range (93). This raises serious difficulties in colliding-beam measurements, owing to the need for distinguishing between multiquantum annihilation (MA) and processes of the double bremsstrahlung (DB) type (see Fig. 10), which contain an electron-positron pair in the final state. These processes have nondecreasing cross sections and occur mainly at scattering angles $\vartheta \sim m/s^{1/2}$ (2). The total cross section (50) exceeds (87) at energies $s^{1/2} \sim 1$ GeV (Table I). Without loss to the DL contribution in MA, it is possible to cut out small angles $\vartheta \sim m/s^{1/2}$ and measure the production of two photons at angles (93). This will result in the loss of one power in the DB cross section. For estimating purposes it can be assumed that the DB cross section at photon emission angles (93) is of the order of the total cross section multiplied by $m/s^{1/2}$. In this case, as seen from Table I, the DB cross section begins to exceed the MA cross section at energies $s^{1/2} \sim 3$ GeV. At high energies, it is necessary to measure the scattered electron-positron pair at angles $\vartheta \sim m/s^{1/2}$ to distinguish the MA from the DB.

TABLE I. Cross sections of electromagnetic processes

| $\sigma_{tot}$, cm² | $s^{1/2}=2E$, GeV | | | | | Formula for cross section |
|---|---|---|---|---|---|---|
| | 1 | 3 | 10 | 100 | 1000 | |
| $\ln(s/m_l)$ | 15.2 | 17.4 | 20.6 | 24.4 | 29.0 | |
| $e^+e^-\gamma$, $\omega_{min}\sim m$ | $10^{-25}$ | $10^{-25}$ | $2\cdot10^{-25}$ | $2\cdot10^{-25}$ | $3\cdot10^{-25}$ | (46) |
| $e^+e^-2\gamma$, $\omega_{min}\sim m$ | $10^{-27}$ | $10^{-27}$ | $10^{-27}$ | $10^{-27}$ | $10^{-27}$ | (50) |
| $e^+e^-e^+e^-$ | $3\cdot10^{-27}$ | $3\cdot10^{-27}$ | $6\cdot10^{-27}$ | $10^{-26}$ | $2\cdot10^{-26}$ | (53) |
| $e^+e^-\mu^+\mu^-$ | | $10^{-32}$ | $7\cdot10^{-32}$ | $10^{-31}$ | $2\cdot10^{-31}$ | (53) |
| $2\gamma$ | $3\cdot10^{-30}$ | $3\cdot10^{-31}$ | $4\cdot10^{-32}$ | $5\cdot10^{-34}$ | $6\cdot10^{-36}$ | (88), (91) |
| $3\gamma$ | $10^{-30}$ | $10^{-31}$ | $2\cdot10^{-32}$ | $3\cdot10^{-34}$ | $6\cdot10^{-36}$ | (92) |
| $\mu^+\mu^-$ | $10^{-31}$ | $10^{-32}$ | $10^{-33}$ | $10^{-35}$ | $10^{-37}$ | (94) |
| $e^+e^-$, $d\sigma/d\Omega$, $s=\lvert t\rvert=\lvert u\rvert$ | $10^{-31}$ | $10^{-32}$ | $10^{-33}$ | $10^{-35}$ | $10^{-37}$ | (41) |
| $e^+e^-$, $\mu^+\mu^-$, $d\sigma/du$, $u\sim m^2$ | $10^{-37}$ | $10^{-39}$ | $10^{-41}$ | $10^{-45}$ | $10^{-49}$ | (96) |

It is also possible to increase, at a fixed energy, the number of registered photons. Then the bremsstrahlung cross section will decrease with each new photon by a factor $\alpha$, and in the MA each $\alpha$ will be cancelled by a double logarithm. At any specified energy it is possible to obtain the number of registered photons at which the MA cross section exceeds the DB cross section.

Another method of separating the MA and DB cross sections is to measure the photon polarizations. The cross section for MA with emission of two photons whose polarization is perpendicular to the $(\mathbf{p}_1, \mathbf{k})$ plane and an indeterminate number of other photons is equal to one-quarter of expression (88). At energies $\omega \ll s^{1/2}$ of the photons making the principal contribution to (50), the bremsstrahlung photons in the DB have a polarization (49) which is longitudinal relative to the momenta $p_1$ and $p_2$.

In addition to the DB, production of several photons with nondecreasing cross section can also occur via the mechanism of the diagram of Fig. 11, with production of $\pi^0$ mesons and subsequent decay of the latter into photons. However, the cross section of this process becomes equal to the MA cross section at energies $s^{1/2} \gtrsim 100$ GeV. Apparently the only way of distinguishing these processes from the process of Fig. 11 is to register the final electrons and positrons down to exceedingly small angles, corresponding to $t \sim m^4/s$, which, as we have seen, make the main contribution to the cross section of the process in Fig. 11.[19]

2) In analogy with multiquantum annihilation, we can obtain the DL asymptotic cross sections for annihilation into a muon pair with emission of an arbitrary number of photons. Diagrams for the cross section of this process are of the same form as in Fig. 13i, with a truncated muon loop with $\delta$ functions inserted in one of the ladder or bremsstrahlung photon (joining different electron lines) in place of the muon propagators. Each of the diagrams 13i must be summed over all possible positions of this loop. The contribution of the bremsstrahlung photons emitted not only by the electrons but also by the muons is cancelled out, just as in the case of multiphoton annihilation, as a result of the emission of an infinite number of real bremsstrahlung quanta. We present only the expression for this process with production of a muon pair only by a ladder quantum[55,56][20]:

$$\sigma_{2\mu,\,n\gamma}^{\perp}=\sigma_{2\mu}^{(0)}\operatorname{ch}x,\quad x=(2\alpha/\pi)\ln(s/m_e^2)\ln(s/m_\mu^2),$$
$$\sigma_{2\mu}^{(0)}=(4\pi\alpha^2/3)\,1/s,\quad d\sigma_{2\mu}^{(0)}/dt=(4\pi\alpha^2/s^4)(t^2+u^2)/2. \qquad (94)$$

Formula (94) is valid at least accurate to terms of order $[\alpha\ln^2(m_\mu^2/m_e^2)]^2$. The first Born term in the expansion of (94) in $\alpha$ corresponds to the absence of ladder photons, the second to the emission of one such photon, the third to emission of two ladder photons, etc. Since the differential cross section of mesic annihilation in the Born approximation is $d\sigma_{2\mu}^{(0)} \sim dt/s^2$ (94), the principal contribution to the first term of (94) is made by $u \sim t \sim s$, i.e., muon emission angles $\vartheta \sim 1$. At the same time, the principal contribution to the second, third, etc. terms of (94) with the additional photons is made by the muon-pair energies $s_\mu$ satisfying the inequality

$$s \gg s_\mu \sim t_\mu \gg m^2.$$

Such values of $t_\mu$ correspond to muon emission angles

of the type (93). If we measure muon emission angles $\vartheta \sim 1$, then all the DL terms vanish ($s_\mu \sim s$) and the muon annihilation cross section coincides with the Born term $\sigma_{2\mu}^{(0)}$. If we measure the angle region (93), then the contribution of the Born diagram turns out to be negligibly small and only the second, third, etc. terms remain in (94). We can also obtain the cross section for $e^+e^-$ annihilation into two or more muon pairs, accompanied by emission of an arbitrary number of photons[56].

Related to the muon annihilation process are processes of annihilation into hadrons. Formula (94) can also be applied to these processes, if the Born cross section for annihilation into hadrons is proportional to 1/s, in analogy with $\sigma_{2\mu}^{(0)}$. If the Born cross section decreases more rapidly than 1/s, as is the case in the production of $\rho$, $\omega$, and $\varphi$ resonances, then the main contribution is determined by diagrams with emission of one or several magnetic photons, in which the hadron loop can be in the resonant region. The principal terms of such diagrams were calculated in[57], and the corresponding cross section for $\rho^0$-meson production is of the order of $10^{-34}$ cm$^2$.

The process of annihilation into a $\mu^+\mu^-$ pair also has a serious competitor, namely the production of a $\mu^+\mu^-$ pair with the aid of the mechanism of Fig. 11. This last process, however, is strongly suppressed because of the presence of the muon mass in the denominator of $r_0^2$. The total cross sections of both processes begin to coincide at energies $s^{1/2} \sim 3$ GeV (Table II). Therefore at energies $s^{1/2} \sim 3$–5 GeV the cross section of the processes of annihilation into a $\mu^+\mu^-$ pair in the DL region $1 \gg \vartheta \gg m/s^{1/2}$ exceeds the $\mu^+\mu^-$ production process. Simultaneous emission of photons in the annihilation process greatly extends the energy region in which this process predominates. In the region of very high energies, apparently the only method of separating this process, just as in the cross section of multiquantum annihilation, is registration of the polarization of the accompanying $\gamma$ quanta or the scattered electrons and positrons.

d) **Scattering through small angles and angles close to 180°.** In addition to the cross sections for multiphoton and muon annihilation, ladder photons contribute also to processes of scattering through very small angles $\vartheta \sim m/s^{1/2}$ ($t \sim m^2$) and angles close to 180° ($u \sim m^2$).

1) The process $e^+e^- \to \mu^+\mu^-$—annihilation forward, i.e., through small angles, is described by a sum of ladder diagrams for the amplitude, of the type of Fig. 15, with the right-hand electron line replaced by a muon line. By small angles is meant here a region in which the definite charge in the reaction does not change its direction: $\mu^-$ ($\mu^+$) moves in the direction of $e^-$ ($e^+$). Just as in the MA case, there is no DL contribution of the bremsstrahlung in this process, this being a direct physical consequence of the rectilinear motion of the charges in the process of the reaction. The amplitude of the process for zero angle is given by (90). The cross section, which is valid at $t \gtrsim m^2$, is[3]

$$d\sigma = d\sigma^{(0)}\,(4/x^2)\,I_1^2(x), \quad x^2 = (2\alpha/\pi)\ln^2(s/t), \quad t \gg m_\mu^2, \qquad d\sigma^{(0)} = (2\pi\alpha^2/s^2)\,dt. \tag{95}$$

The cross section (95) differs from the Born cross section only at $t \sim m_\mu^2$ ($\vartheta \sim m_\mu/s^{1/2}$). In this case $dt \sim m_\mu^2$ and $d\sigma^{(0)} \sim 4\pi\alpha^2 m_\mu^2/s^2$, i.e., it decreases quadratically with increasing s.

2) Electron-positron backward scattering ($u \sim m^2$) contains a DL contribution from ladder diagrams with electron lines directed to one side of Fig. 13i. In this case, the two colliding charges reverse their directions of motion. This causes powerful bremsstrahlung, manifest in the fact that the DL contribution is made by diagrams with bremsstrahlung photons that are inserted in arbitrary fashion in the ladder sequence of Fig. 13i, and the contributions of photons joining one and the same or different electron lines in Fig. 13i are additive. These bremsstrahlung photons are emitted, as before, independently of one another, and the result is an exponential form that depends on the variables of the main process (in this case—the ladder).

Summation of all the diagrams leads to an equation of the type (84) with an exponential kernel, the solution of which leads to a cross section in the form[3]

$$d\sigma = d\sigma^{(0)} J^2(x_u), \quad x_u^2 = (2\alpha/\pi)\ln^2(s/u), \quad u \gg m_e^2, \tag{96}$$

$$d\sigma^{(0)} = (4\pi\alpha^2/s^2)\,du, \quad J(x) = (2i/\pi)\int_{a-i\infty}^{a+i\infty} e^{lx}\,(\partial/\partial l)\ln D_{-1/4}(l)\,dl,$$

$$J(x) = \begin{cases} 1-(5/8)\,x^2+(35/192)\,x^4+\ldots, & x \ll 1; \\ -8\,[e^{-2,26x}\cos 1.84x + e^{-3.44x}\cos 3.05x + \ldots], & x \gg 1, \end{cases} \tag{97}$$

where $D_{-1/4}(l)$ is a parabolic-cylinder function.

The function J(x) differs from one at large $x_u^2 \sim 1$, i.e., at scattering angles $\pi - \vartheta \lesssim m/s^{1/2}$. Formula (96) is also valid for the process $e^-e^+ \to \mu^-\mu^+$—backward annihilation at $u \gtrsim m_\mu^2$. At very high energies, $x_u^2 = (2\alpha/\pi)\ln^2(s/u) \gg 1$, the amplitude (98) takes the form of rapidly damped oscillations.

As already mentioned, in order for the DL contribution to (95) and (96) to be significant, it is necessary to consider very small forward or backward scattering angles, at which $-t \sim m^2$ or $-u \sim m^2$ ($dt \sim du \sim m^2$). The Born term in (95) and (96) is equal to $4\pi\alpha^2 m^2/s^2$. At $s^{1/2} \sim 1$ GeV, this quantity is of the order of $10^{-37}$ cm$^2$ (see Tables I and II). With the VÉPP-2′ installation having transmissions on the order of $10^{32}$ sec$^{-1}$ cm$^{-2}$, processes with such a cross section will occur approximately once every 3–4 days. The DL contribution increases somewhat the cross section of the process (95) and decreases the cross section of the process (96) (see Table II). At $s^{1/2} \sim 1$ GeV, the cross section for $e^+e^-$ backward scattering is one-quarter of the Born term and occurs in the VÉPP-2 apparatus approximately once every two weeks instead of once every 3–4 days.

3) Formula (96), like all the preceding formulas, is valid in the case of emission of an arbitrary number of bremsstrahlung photons with $-k_\perp^2 \ll m^2$. This corresponds to a scattered-particle noncollinearity angle $\Delta\vartheta = k_\perp/s^{1/2} \lesssim m/s^{1/2}$. When bremsstrahlung photons with large $-k_\perp^2 \gg m^2$ are emitted, there is no cancellation of the contributions of the virtual and real bremsstrahlung photons (just as in the total cross section of multiphoton

TABLE II. Energy dependence of the doubly logarithmic asymptotic cross sections

| $\sigma/\sigma_0$ | $s^{1/2} = 2E$, GeV | | | | | Cross section formula |
|---|---|---|---|---|---|---|
| | 1 | 3 | 10 | 100 | 1000 | |
| $(2\alpha/\pi)\ln^2(s/m_l^2)$ | 1 | 1.4 | 2 | 3 | 4 | |
| $(2\alpha/\pi)^{1/2}\ln m_l^{-2}$ | 1.03 | | 1.41 | 1.68 | 1.98 | |
| $\sigma_{\infty\gamma}/\sigma_{2\gamma}^{(0)}$ | 1.09 | | 1.15 | 1.20 | 1.38 | (87) |
| $\sigma_{2\mu,\,\infty\gamma}/\sigma_{2\mu}^{(0)}$ | 1.19 | | 1.48 | 1.86 | 2.44 | (94) |
| $d\sigma_{e^+e^-}/d\sigma_{e^+e^-}^{(0)}$, $u \sim m^2$ | 0.25 | 0.19 | 0.092 | 0.040 | 0.0058 | (96) |

annihilation). The reason is that the photons with large $k_\perp$ are not classical, and the kinematics of the process changes when they are emitted. We put

$$u_1=(p_1-p_2')^2, \quad u_2=(p_2-p_1')^2.$$

In the case of emission of bremsstrahlung photons with large $k_\perp^2 \gg m^2$ and $u_1 \neq u_2$, it is possible to obtain the differential cross section of the process with emission of a given number n of bremsstrahlung photons, integrated over all $u_2$ at fixed $u_1 \sim m^2$. This cross section is in general rather complicated in form [49]. In the case of not too large energies ($(\alpha/\pi)\ln^2(1/m^2 \ll 1$) and very high energies ($(\alpha/\pi)\ln^2(s/m^2) \gg 1$), this cross section takes the form [49]

$$\frac{d\sigma_n}{du_1}=\begin{cases}\dfrac{d\sigma^{(0)}}{du_1}\dfrac{(2x^2)^n}{(2n)!}, \quad x^2=\dfrac{2\alpha}{\pi}\ln^2\left(\dfrac{s}{u_1}\right), & x\ll 1,\\ \dfrac{d\sigma^{(0)}}{du_1}0.773\dfrac{(0.762)^n}{(n-1)!}\dfrac{1}{x}[\ln^{n-1}x+O(\ln^{n-2}x)], & x\gg 1.\end{cases} \tag{98}$$

Summation of formula (98) over n, with allowance for all (not only the higher-order) logarithms, yields in the case of ultrahigh energies [49]

$$d\sigma/du_1 = 0.78\, d\sigma^{(0)}/du_1, \quad x^2=(2\alpha/\pi)\ln^2(s/u_1)\gg 1. \tag{99}$$

The ratio of the cross section of the electron-positron backward scattering with emission of bremsstrahlung photons (98) to the Born term decreases with increasing energy (like $1/\ln(s/u_1)$), in contrast to the process without photon emission (96) and (97), for which this ratio decreases exponentially. Summation over the number of bremsstrahlung photons n causes the indicated ratio to assume the constant value (99).

The author is grateful to V. N. Baĭer, L. F. Ginzburg, V. N. Gribov, L. N. Lipatov, É. A. Kuraev, V. G. Serbo, G. V. Frolov, and V. A. Khoze for a number of valuable remarks and advice.

[1)] All the formulas that follow are valid accurate to terms of order $m^2/s$.

[2)] The terms "parallel" and "series" are analogs of the terms used in electrical circuits.

[3)] For simplicity we have shown in Fig. 4 an amplitude $M^n$ consisting of the simplest pole diagrams that depend on the momentum transfers in the t-channel [22,23], but our analysis can also be used for an arbitrary form of $M^n$.

[4)] The possible appearance of only logarithmically large quantities after integration over the phase volume is a specific feature of electrodynamic perturbation theory, as will be verfied below.

[5)] This statement is valid only within the framework of perturbation theory, when all the amplitudes are described by Born terms, i.e., by Feynman diagrams with the smallest number of virtual particles. At very high energies, when the effective parameters of perturbation theory are large, $\alpha \ln^2(s/m^2) \gg 1$ or $\alpha \ln(s/m^2) \gg 1$, the summation of the perturbation-theory series can change the behavior of the amplitude appreciably (see Chap. 4).

[6)] In the c.m.s. of the t-channel we have $p_1 - p_1' = 0$, $s = -(t/2)(1 - \cos\nu)$, whence $\cos\nu = (2s/t) + 1 \approx 2s/t$, $s \gg t$.

[7)] In the case of a constant asymptotic amplitude produced upon exchange of two spinor particles ($\sigma_1 + \sigma_2 = 1$), the contribution from small $t' \sim t \sim m^2$.

[8)] For example, the summation of diagrams of type 5b with all possible permutations of the photon lines leads in the logarithmic approximation to an additional multiplication of the first diagram with one photon in the t-channel by the Coulomb phase $\exp(i\alpha \ln t/\lambda^2)$ ($\lambda$ is the photon mass), which contains only ln t and makes no contribution to the cross section.

[9)] The Feynman diagram obtained for the elastic-scattering amplitude from Fig. 9b by replacing the crossed lines by ordinary propagators has a three-photon splitting and is proportional to s. This is connected with the presence in this diagram of other imaginary parts corresponding to the processes without photon emission. They are radiative corrections to the elastic scattering of an electron by a positron and electron.

[10)] Doubling (49) in accordance with the emission of the electron and positron, expanding the integral with respect to $d\omega$ in terms of $t'$, and multiplying the result by the Rutherford cross section (37) we arrive at formula (44) [35].

[11)] If the diagrams of Fig. 13 constitute an internal part of a complicated Feynman diagram with virtual electron line momenta $q_1$, $q_2$ and $q_1'$, $q_2'$ (12), satisfying conditions of the type of (57) as before, then diagram 13b is of the order of $\alpha \ll 1$ or $\beta \ll 1$ relative to the diagram 13a, which is equivalent only to logarithmic smallness.

[12)] For the virtual bremsstrahlung photon in Fig. 13c or 13d, a DL contribution is made in different regions of the variables (59) also by the poles of the electron propagators, but the summary contribution coincides with the contribution of one photon pole within the limits of (62).

[13)] Obviously, photons with $-k_\perp^2 \sim m^2$ ($\lambda = 0$) do not lead to a DL contribution (see Fig. 14).

[14)] At energie $s^{1/2}$ above 550 GeV, the Born term of the processes $e^+e^- \to e^+e^-$ and $e^+e^- \to$ neutral leptons at $s \sim |t| \sim |u|$ will be determined no longer by electromagnetic but by weak interaction the amplitudes of which increase with increasing energy like $(Gs)^2$. $G \approx m_p^{-2} \times 10^{-5}$. [52]

[15)] For the process $ee \to \mu\mu$ it is necessary to replace a by the sum of two terms with $m = m_e$ and $m = m_\mu$.

[16)] In [3] we solved the equation obtained from (84) by substituting $\rho - \xi = \eta'$ and $\rho - \eta = \xi'$.

[17)] The cross section for two quantum annihilation with production of one ladder photon and one bremsstrahlung photon is determined by the imaginary part of the diagram 13g. In view of the independence of the emission (the Poisson character) of the bremsstrahlung photons in the DL approximation, this cross section is proportional to the imaginary part of the pole diagram 13a (77), and is equal to zero.

[18)] In the case of cutoff of the soft photons, under the condition $\omega_{min} \sim m$ (67), the value of $\sigma_{3\gamma}^{(0)}$ (92) is doubled [15], as can be verified easily with the aid of Fig. 14.

[19)] When ordinary accelerators with immobile target are used, the registration of the final positrons and their separation from the electrons of the initial beam are possible at all angles.

[20)] The muon pairs produced by the ladder photon have only perpendicular momenta of the initial particles of the muon-current component $j_\mu^\perp = u_{\mu+}\gamma_\mu^\perp u_{\mu-}$. It is a difficult matter to separate them from muon pairs produced by a bremsstrahlung photon with parallel component of the current $j_\mu$. However, the contribution of the pairs produced by a bremsstrahlung photon arises when not fewer than two real ladder photons are emitted simultaneously (in forth-order perturbation theory), and is numerically small. It should increase the cross section (94), somewhat since there is no interference between $\mu$-pair production by bremsstrahlung and ladder photons.

[1] V. N. Gribov, Lektsii po teorii kompleksnykh momentov (Lectures on the Theory of Complex Momenta), KhFTI Preprint 70/47, Khar'kov, 1970.
[2] H. Cheng and T. T. Wu, Phys. Rev. **182**, 1852, 1868, 1873, 1899 (1969).
[3] V. G. Gorshkov, V. N. Gribov, L. I. Lipatov, and G. V. Frolov, Yad. Fiz. **6**, 129, 361, 579 (1967) [Sov. J. Nucl. Phys. **6**, 95, 262, 461 (1967)].
[4] M. Gell-Mann, M. L. Goldberger, F. E. Low, E. Marx and F. Zachariasen, Phys. Rev. **B133**, 145 (1964).
[5] G. V. Frolov, V. G. Gorshkov, and V. N. Gribov, Phys. Lett. **22**, 662 (1966); L. N. Lipatov, Zh. Eksp. Teor. Fiz. **54**, 1520 (1968) [Sov. Phys.-JETP **27**, 814 (1968)].
[6] H. Cheng and T. T. Wu, Phys. Rev. Lett. **22**, 666 (1969).
[7] L. N. Lipatov and G. V. Frolov, ZhETF Pis. Red. **10**, 399 (1969) [JETP Lett. **10**, 254 (1969)].
[8] G. V. Frolov, V. N. Gribov and L. N. Lipatov, Phys. Lett. **B31**, 34 (1970); **12**, 994 (1970).
[9] H. Cheng and T. T. Wu, Phys. Rev. Lett. **23**, 670 (1969).
[10] C. Weizsacker, Zs. Phys. **88**, 612 (1934); E. Williams, Phys. Rev. **45**, 729 (1934).
[11] V. N. Gribov, V. A. Kolkunov, L. B. Okun' and V. M.

Shekhter, Zh. Eksp. Teor. Fiz. **41**, 1315 (1961) [Sov. Phys.-JETP **14**, 935 (1962)].
[12] L. Landau and E. Lifshitz, Sov. Phys. **6**, 244 (1934).
[13] V. V. Sudakov, Zh. Eksp. Teor. Fiz. **30**, 87 (1956) [Sov. Phys.-JETP **3**, 65 (1956)].
[14] A. A. Abrikosov, ibid., pp. 386, 544.
[15] B. V. Geshkenbeĭn and M. B. Terent'ev, Yad. Fiz. **8**, 119 (1968) [Sov. J. Nucl. Phys. **8**, 67 (1969)].
[16] S. Okubo, Nuovo Cimento **18**, 70 (1960); K. E. Erikson, ibid. **19**, 1010 (1961); P. R. Yenni, S. C. Frautschi and U. Suura, Ann. Phys. (N.Y.) **13**, 379 (1961).
[17] V. N. Baĭer and S. A. Kheifets, Zh. Eksp. Teor. Fiz. **40**, 613 (1961) [Sov. Phys.-JETP **13**, 428 (1961)].
[18] G. A. Milekhin and E. S. Fradkin, Zh. Eksp. Teor. Fiz. **45**, 1926 (1963) [Sov. Phys.-JETP **18**, 1323 (1964)].
[19] V. N. Baĭer, Usp. Fiz. Nauk **78**, 619 (1962) [Sov. Phys.-Uspekhi **5**, 976 (1963)].
[20] A. I. Alikhan'yan and S. A. Kheifets, Usp. Fiz. Nauk **101**, 217 (1970) [Sov. Phys.-Uspekhi **15**, 353 (1970)].
[21] W. E. Thirring, Principles of Quantum Electrodynamics, Academic, 1958 (Russ. transl., Vysshaya shkola, 1964, p. 150).
[22] D. Amati, S. Fubini and A. Stanghellini, Nuovo Cimento **26**, 896 (1962).
[23] I. M. Dremin, I. I. Roĭzen, R. B. Uait, and D. S. Chernavskiĭ, Zh. Eksp. Teor. Fiz. **48**, 952 (1965) [Sov. Phys.-JETP **21**, 633 (1965)].
[24] S. Mandelstam, Phys. Rev. **112**, 1344 (1958).
[25] R. E. Cutkosky, J. Math. Phys. **1**, 429 (1960).
[26] A. M. Popova and K. A. Ter-Martirosyan, Nucl. Phys. **60**, 607 (1964).
[27] Ya. I. Azimov, Zh. Eksp. Teor. Fiz. **43**, 2321 (1962) [Sov. Phys.-JETP **16**, 1639 (1963)].
[28] S. Mandelstam, Nuovo Cimento **30**, 1113, 1127, 1143 (1963).
[29] A. G. Khabakhpashev, Preprint IYaF 112-70, SO AN SSSR, Novosibirsk, 1970; V. E. Balakin et al., Phys. Lett. **B34**, 663 (1971).
[30] A. I. Akhiezer and V. B. Berestetskiĭ, Kvantovaya élektrodinamika (Quantum Electrodynamics), Moscow, Nauka, 1969.
[31] H. Bethe and W. Heitler, Proc. Roy. Soc. **146**, 83 (1934).
[32] G. M. Garibyan, Izv. Akad. Nauk Arm. SSR **5**, 3 (1952).
[33] J. A. Altarelli and F. Buccella, Nuovo Cimento **34**, 1337 (1964).
[34] V. N. Baĭer, V. S. Fadin and V. A. Khoze, Zh. Eksp. Teor. Fiz. **51**, 1135 (1966) [Sov. Phys.-JETP **24**, 760 (1967)].
[35] V. N. Baĭer and V. M. Galitskiĭ, Phys. Lett. **13**, 355 (1964); **2**, 259 (1965).
[36] V. N. Baĭer, V. S. Fadin, and V. A. Khoze, Zh. Eksp. Teor. Fiz. **53**, 2194 (1967) [Sov. Phys.-JETP **26**, 1238 (1968)].
[37] É. A. Choban, Yad. Fiz. **13**, 624 (1971) [Sov. J. Nucl. Phys. **13**, 354 (1971)]; A. M. Altukhov, ibid. **14**, 391 (1971) [**14**, 220 (1972)]; V. N. Baĭer and V. S. Fadin, ZhETF Pis. Red. **13**, 293 (1971) [JETP Lett. **13**, 208 (1971)].
[38] V. N. Baĭer and V. S. Fadin, Phys. Lett. **B27**, 223 (1968); V. N. Baĭer and V. A. Khoze, Zh. Eksp. Teor. Fiz. **48**, 1708 (1965) [Sov. Phys.-JETP **21**, 1145 (1965)].
[39] V. S. Synakh, Zh. Eksp. Teor. Fiz. **48**, 1111 (1965) [Sov. Phys.-JETP **21**, 742 (1965)].
[40] V. N. Baĭer and V. S. Fadin, Zh. Eksp. Teor. Fiz. **61**, 476 (1971) [Sov. Phys.-JETP **34**, 253 (1972)].
[41] É. A. Kuraev and L. I. Lipatov, ZhETF Pis. Red. **15**, 229 (1972) [JETP Lett. **15**, 159 (1972)]; Yad. Fiz. **16**, 1060 (1972) [Sov. J. Nucl. Phys. **16**, 584 (1973)].
[42] S. J. Brodsky, T. Kinoshita and H. Terazawa, Phys. Rev. Lett. **25**, 972 (1970).
[43] G. V. Meledin, V. G. Serbo and A. I. Slivkov, ZhETF Pis. Red. **13**, 98 (1971) [JETP Lett. **13**, 68 (1971)].
[44] V. G. Serbo, ibid. **12**, 50 (1970) [**12**, 39 (1970)].
[45] L. I. Lipatov and G. V. Frolov, a) Materialy, predstavlennye na 15-uyu Mezhdunarodnuyu konferentsiyu po fizike vysokikh énergii (Materials presented at the Fifteenth International Conference on High-Energy Physics), Kiev, 1970; b) Yad. Fiz. **13**, 588 (1971) [Sov. J. Nucl. Phys. **13**, 333 (1971)].
[46] F. E. Low, Phys. Rev. **120**, 582 (1960).
[47] V. M. Budnev and A. I. Slivkov, ZhETF Pis. Red. **12**, 523 (1970) [JETP Lett. **12**, 367 (1970)].
[48] V. E. Balakin, V. M. Budnev, and I. F. Ginzburg, see ref. 45a; V. M. Budnev and I. F. Ginzburg, Preprint TF-55, SO AN SSSR, Novosibirsk, 1970; ZhETF Pis. Red. **13**, 519 (1970) [JETP Lett. **13**, 370 (1971)]; M. V. Terent'ev, Yad. Fiz. **14**, 178 (1971) [Sov. J. Nucl. Phys. **14**, 99 (1972)]; É. A. Choban and V. M. Shekhter, ibid. **19**, 190 (1974) [**19**, No. 1 (1974)].
[49] L. N. Lipatov, Yad. Fiz. **6**, 564 (1967) [Sov. J. Nucl. Phys. **6**, 411 (1967)]; ibid. **14**, 396 (1971) [**14**, 223 (1972)].
[50] V. N. Gribov, ibid. **5**, 399 (1966) [**5**, 280 (1966)].
[51] V. G. Gorshkov, Zh. Eksp. Teor. Fiz. **56**, 597 (1969) [Sov. Phys.-JETP **29**, 329 (1969)].
[52] A. D. Dolgov, V. I. Zakharov, and L. B. Okun', Yad. Fiz. **14**, 1044, 1247 (1971) [Sov. J. Nucl. Phys. **14**, 585, 695 (1972)].
[53] V. G. Gorshkov and L. N. Lipatov, Yad. Fiz. **9**, 818 (1969) [Sov. J. Nucl. Phys. **9**, 480 (1969)].
[54] É. A. Kuraev and A. I. Kalinchenko, ibid. **12**, 122 (1970) [**12**, 68 (1971)].
[55] Yu. I. Ol'shanskiĭ, Diploma Thesis (LPI, Leningrad, 1970).
[56] É. A. Kuraev, M. M. Nesterov, and Yu. I. Ol'shanskiĭ, Yad. Fiz. **13**, 825 (1971) [Sov. J. Nucl. Phys. **13**, 471 (1971)].
[57] É. A. Choban, ZhETF Pis. Red. **11**, 505 (1970) [JETP Lett. **11**, 346 (1970)].

Translated by J. G. Adashko